INTRACELLULAR LOCALIZATION, BIOCHEMICAL AND BIOPHYSICAL PROPERTIES OF HUMAN ARMET

by

XIAOXI ZHU

B.A., Southwest University of Science and Technology, China, 2007

A THESIS

submitted in partial fulfillment of the requirements for the degree

MASTER OF SCIENCE

Department of Biochemistry
College of Art and Sciences

KANSAS STATE UNIVERSITY
Manhattan, Kansas

2011

Approved by:

Major Professor
Gerald Reeck

Abstract

Armet is a bifunctional protein widely distributed in animal species, vertebrate and invertebrate. It is an evidently part of the Unfolded Protein Response (UPR) and promotes survival in cells that are under endoplasmic-reticulum (ER) stress. It has also been found as a secreted protein with neurotrophic activity. The crystal and solution structures of human Armet show it is a helix-rich protein with two domains linked through a flexible linker region. In this study, immunofluorescence staining was used to verify Armet's localization in ER and Golgi apparatus in MBA-MD-231 cells. Evidence for calcium binding by Armet was obtained by circular dichroism spectroscopy (the binding of calcium appeared to decrease helix content), by differential scanning calorimetry (binding of calcium resulted in a less structured protein) and two-dimensional (^{1}H-^{15}N HSQC) nuclear magnetic resonance spectroscopy. A difference HSQC spectrum of Armet, with and without calcium, showed peaks of increased intensity, of decreased intensity and of perturbed chemical shift. There were about 30 such peaks in total. Several of these affected amino acid residues appeared to form a cluster of negatively charged side chains that could possibly form a binding site for a calcium ion. Heterogeneity of three types was observed in recombinant Armet expressed in *E. coli* cells. Two bands of slightly different mobility were observed in SDS gels run in the absence of reducing agent. These may represent alternate arrangements of disulfide bonds, as previously reported by other investigators but not explained. Further, in the absence of reducing agent, a faint ladder was formed by human Armet, indicating formation of disulfides between Armet molecules. Oligomers with sedimentation coefficient greater than the monomeric protein, in the absence of reducing agent, disappeared in the presence of a reducing agent. Finally, minor species of mass differences of 98 and 180 with respect to the main protein component were observed by MALDI-TOF mass spectrometry.

These studies provide a more thorough characterization of Armet than has been previously available and set the scene for future investigations of the binding of organic ligands to the protein.

Table of Contents

List of Figures

List of Tables

Acknowledgements

I would like to express my deepest gratitude to my major professor, Dr. Gerald Reeck, for his patient guidance throughout my graduate study. I would also like to thank Dr. Qize Wei and Dr. Om Prakash for serving on my committee and helping me with my research. I thank Dr. Michael Kanost, Dr. John Tomich, and Dr. Michal Zolkiewski for letting me use instruments in their labs. Many thanks to Dr. Daisuke Takahashi for collecting 2D ^{1}H-^{15}N HSQC data. I also want to thank Dr. Yasuaki Hiromasa for data collection and analysis of mass spectrometry and ultracentrifuge data. Thanks to Dr. Changzhong Sheng, Dr. Di Wu, Dr. Feng Cui, and Ting Zhang for helping me with experiments. Finally, I want to say thank you to every member in my family. They are at all times my greatest support, inspiration and encouragement.

Chapter 1 - Introduction

Armet: the protein and its names

A cDNA encoding a protein with 234 amino residues was identified from human chromosomal band 3p21.1 (Shridhar et al., 1996). The encoded protein was first named arginine-rich protein (ARP) because it appeared to contain 22 arginines in the first 55 residues. This protein was also believed to be "mutated in early stage of tumors" and was therefore named Armet when mutants if it were found in a variety of cancers such as head and neck, lung, breast, prostate, and pancreatic cancers (Shridhar et al., 1996, 1997). However, a later study (Evron et al., 1997) showed that the variations of ARP's sequence in tumors represented normal polymorphisms rather than tumor-specific mutations. Since the name "Armet" was kept and still used in later publications, it will be used in this thesis.

Armet protein was not purified or cloned until 2003. Petrova et al. (2003) isolated a neurotrophic factor secreted by human ventral mesencephalic cell line 1 (VMCL1), which was partially identical in sequence to Armet but only contained 179 residues. It was then clear that the originally predicted arginine-rich region of the transcript was not translated. Armet was instead secreted after cleavage of a 21 residue, N-terminal signal peptide. Petrova et al. (2003) gave Armet the alternative name of mesencephalic, astrocyte-derived neurotrophic factor (MANF) (Petrova et al., 2003). Glycosylation of Armet expressed in HEK293 cells was reported (Petrova et al., 2003), but in later studies (Mizobuchi et al., 2007; Lindholm et al., 2008), modified human and mouse Armet were not detected.

Unfolded protein response (UPR)

Endoplasmic reticulum (ER) is an important organelle for nascent secretory and transmembrane protein folding and posttranslational modification. When the physiological homeostasis of ER is perturbed, signal pathways will be activated to increase the biosynthetic capacity and decrease the biosynthetic burden. And these pathways are called UPR (Ma et al., 2004, Schroder et al., 2005, Kim et al., 2008). The unfolded proteins are recognized by Bip, UGGT and other less known ER chaperones. Binding of unfolded protein and chaperones activates three ER membrane proteins: PERK, IRE1, and ATF6 (Schroder et al., 2005).

Phosphorylation of eIF-2α by PERK results in general inhibition protein synthesis. IRE1 causes the mRNA splicing of XBP1, which is an important transcription factor regulating expression of gene in ER stress. Activation of ATF6 upregulates chaperone expression (Ma et al., 2004).

Armet's function in ER stress

Several studies have indicated that Armet is a part of the UPR during ER stress induced cell death (Mizobuchi et al., 2007, Apostolou et al., 2008, Tadimalla et al., 2008, Hellman et al., 2010, Yu et al., 2010). Armet's gene was first found to be ER-stress-induced from expression microarray analysis (Apostolou et al., 2008). Knockdown of Armet mRNA by siRNA treatment of Hela cells rendered the cells more susceptible to ER stress-induced death. Overexpression of Armet improved cell viability under glucose-free starvation and in ER stress (Apostolou et al., 2008). Armet levels were detected to be increased by tunicamycin and thapsigargin induced ER stress along with another well-known ER stress response protein, Grp78 (Bip) (Apostolou et al., 2008), Armet's mRNA and protein expression patterns were similar to Grp78's (Mizobuchi et al., 2007).

In ischemia, ER stress leads to protein misfolding caused by the low oxygen level (Kumar et al., 2001; Paschen et al., 2003; Morimoto et al., 2007; Oida et al., 2008; Yu et al., 2010). Protein level of Armet was found to be increased by cerebral ischemia (Apostolou et al., 2008; Yu et al., 2010). An increased Armet mRNA level was detected along with induced protein expression in heart ischemia (Tadimalla et al., 2008). Addition of recombinant Armet in culture medium protected cultured cardiac myocytes from stimulated ischemia/ reperfusion-mediated death (Tadimalla et al., 2008), and injection of recombinant Armet in cerebral cortex reduced ischemic brain injury and promoted behavioral recovery in rats (Airavaara et al., 2009).

Armet's detailed or specific role is not known. For instance, it is not known what binds to Armet. Armet's promoter contains one putative ER stress response element (ERSE) (Tadimalla et al., 2008), and an ERSE-II region which contains two transcription factor recognition sequences for recognition by ATF6/ XBPI, and NF-Y (Mizobuchi et al., 2007; Tadimalla et al., 2008). Human Armet also has a C-terminal RTDL sequence for ER retention(Apostolou et al., 2008).

Armet as a neurotrophic factor (MANF)

As a neurotrophic factor, Armet (MANF) selectively protected nigral dopaminergic neurons, but not GABAergic or serotonergic neurons (Petrova et al., 2003). Armet (MANF) is a homolog to dopamine neurotrophic factor (CDNF) (Lindholm et al., 2007). Receptors of these two proteins are unknown. Later studies suggested Armet (MANF) promotes neuron proliferation (Yu et al., 2010) and protects neurons intracellularly as efficiently as Ku70 (Hellman et al., 2010). Voutilainen et al. (2009) suggest Armet (MANF) to be a new target for Parkinson's disease therapy and their preliminary data has shown its neurorestorative function in a rat model.

Armet's structure

Crystal and solution structures of human Armet, and the solution structure of mouse Armet have been published (Fig. 1.4). The first was obtained by X-ray crystallography and only contained residues 1 to 137 due to the lack of electron density in the C-terminal area. Armet crystallized as a monomer at neutral pH. There are five α-helices followed by a turn of 3_{10} helix in the N-terminal region (residues 1-95). Residues 111-137 of the C-terminal region contain two α-helices and are connected with the N-terminal region by a loop or linker (residues 95-111). Three disulfide bridges formed (Cys6-Cys93, Cys9-Cys82, and Cys40-Cys51) were found in the N-terminal domain. Another (Cys123-Cys130) was found in C-terminal domain (Parkash et al., 2009).

Structural alignment based on crystal structure of Armet suggested that the N-domain had a saposin-like structure, and C-terminal domains have one CXXC motif which is often observed in reductases and disulphide isomerases (Parkash et al., 2009).

Hellman et al. (2010) obtained a solution structure of human Armet by NMR (Fig. 1.5, Fig. 1.6). In this structure, the protein contained three parts: an N-terminal domain (residues 1-95), a linker region (residues 96-103), and a C-terminal domain (residues 104-158). The N-terminal domain contained five α-helices and one 3_{10} helix. The C-terminal domain contained one loosely formed α-helix followed by two parallel α-helices. Eight cysteines in the mature protein all formed disulfide bonds. The arrangement of disulfide bonds was consistent with result obtained in the X-ray crystallography study (Prakash et al., 2009). Low heteronuclear ^{1}H-^{15}N NOE values indicated the linker region, residues 1-4 and residues 148-158 were highly flexible.

The structure of residues 96-158, expressed independently, is identical to the same region in full-length protein (Hellman et al., 2010). No NOE signals were observed between the two domains indicates a relatively high fluctuation between orientations of these two domains or a wide separation between the two domains (Hellman et al., 2010).

Structural superimposition showed the C-domain was structurally similar to members of the SAP (SAF-A/B, Acinus and PIAS) protein superfamily (Hellman et al., 2010). Although Armet and Ku70 share high structural similarity, and have similar protective function toward neurons, it is not clear whether Armet can bind Ku70's ligand, which is Bcl-2-associated X protein (BAX) (Hellman et al., 2010).

The structure of mouse Armet has also been solved by NMR. Mouse Armet has 97% sequence identity with human Armet (Fig. 1.2, Fig. 1.5, Fig. 1.6). The N-terminal domain of mouse Armet is comprised of six helices. Four helices (α_1, α_2, α_4, π) constitute a bundle-like structure followed by α_3 and 3_{10} helices. The π helix is always involved in ligand/enzyme substrates binding. More interestingly, the negatively charged residues in the π-helix are not conserved as other positively charged residues on other part of the N-domain. Signal broadening in the HSQC spectrum indicates the linker region is flexible. ^{15}N spin-relaxation parameters suggest N- and C- domains are connected by a flexible linker and tumble independently (Hoseki et al., 2010). These observations agree with the NMR study of human Armet (Hellman et al., 2010). Four disulfide bounds were found in the NMR study of mouse Armet and the result was verified by MALDI-TOF MS. But in an earlier MALDI-TOP MS study of mouse Armet (Mizobuchi et al., 2007), C6 formed a disulfide bond with C9 instead of C93, and C93 formed a disulfide bond with C82. This indicates the possible heterogeneity of disulfide bond arrangement in Armet.

ER stress and cancer

Poorly vascularized solid-tumor cells encounter a range of cytotoxic conditions such as hypoxia and nutrient starvation which alter the physiological environment of the ER. Accumulation of misfolded protein in the ER will activate the UPR (Ma et al., 2004). *In vitro* activation of the UPR decreases the sensitivity of cancer cells to treatments (Ma et al., 2004) (Healy et al., 2009). It is known that UPR is activated in breast tumors (Fernandez et al., 2000), hepatocellular carcinomas (Shuda et al., 2003), and gastric tumors (Song et al., 2001) with up-

regulation of ER chaperones such as Grp78. XBP1, an ER stress-induced protein was reported to be necessary to tumor growth *in vivo* (Romero-Ramirez et al., 2004). More comprehensive studies need to be done to identify which component is most important in relative pathways, how large a role the UPR has in tumor growth, and at which stages of tumor development are regulated by UPR proteins. Although Armet is involved in reacting to ER stress, nothing is known about how it interacts with other components in UPR signaling, and how it is important in cancers.

Goal of this study

The research presented in this thesis is intended to provide information on the intracellular localization, biochemical and biophysical properties of human Armet. Such information will contribute to a better understanding of Armet's function and to future studies such as the binding of chemical ligands to Armet.

Chapter 2 - Methods

Recombinant human Armet expression and purification

N-terminal 6X His-tagged human Armet gene without signal peptide was amplified by PCR from plasmid containing C-terminal 6×His-tagged human Armet gene using primers 5'-GCCCATGGGCCACCACCACCACCACCACctgcggccgggcgac-3' and 5'-GGCCCTCGAGCTACAAATCGGTCCG-3'. The PCR product was cloned into pET-28a-c(+) vector using NcoI and XhoI sites. Cloned Armet was confirmed by sequencing. To express protein, *Escherichia coli* strain BL21 (DE3) transformed with the recombinant plasmid was cultured at 37 ℃using LB medium until OD 600 reached 0.6. Induction of the recombinant protein was performed with 1 mM IPTG for 4 hr at 30 ℃. Cells were harvested and resuspended in 50 mM Na_2HPO_4, 300 mM NaCl, 10 mM immidazole, pH 8.5. After sonication, the resulting lysates were centrifuged at 14,000 g for 20 min. The supernatant was loaded on Ni-NTA column. Impurities were eluted by 40 column volume of 50 mM Na_2HPO_4, 300 mM NaCl, 20 mM immidazole. Then N-terminal 6X His-tagged human Armet were eluted by 5 column volume of 50 mM Na_2HPO_4, 300 mM NaCl, 300 mM immidazole followed by dialysis overnight at 4 ℃ with 50 mM Tris-HCl, 100 mM NaCl, pH 7.0.

To express ^{15}N labeled protein, *Escherichia coli* strain BL21 (DE3) transformed with the recombinant plasmid was cultured at 37 ℃using M9 medium (12.8 g $Na_2HPO_4 \cdot 7H_2O$, 3 g KH_2PO_4, 0.25 g NaCl, 1 g $^{15}NH_4Cl$ in 1 L distilled H_2O, autoclaved) with filter sterilized 2ml of 1 M $MgSO_4$, 20 mL of 20 % glucose, 100 uL of 1 M $CaCl_2$ until OD 600 reached 0.6. Induction of the recombinant protein was performed with 1 mM IPTG for 24 hr at 30 ℃.

Western blot analysis

Purified human Armet polyclonal antibody was obtained from R&D Systems (Lot YLB0207081). The antigen was mouse myeloma cell line NS0 derived recombinant human MANF consisted of Leu22-Leu179 and the antibody was raised in goat.

Protein samples were incubated for 5 min in boiling water, and then loaded in a 12% acrylamide gel and run on constant voltage of 80 V for approximately 30 min, and run on

constant voltage of 180 V for another 1 hr. The separated proteins on the gel were transferred on a nitrocellulose membrane using a half-dry transfer cell. The membrane was incubated in 5% instant non-fat dry milk in TBST for 1hr for non-specific protein binding site blocking. The membrane was then incubated with purified anti-human Armet antibody at 1:1000 dilution in TBST containing 5% non-fat dry milk overnight. In the next morning, the membrane was washed with TBST 3 times, at 5 min per wash. The membrane was then incubated with rabbit anti-goat IgG (H+L)-AP conjugate (Bio-Rad Laboratories) at 1:3000 in TBST for 1 hr at room temperature. The membrane was again washed 3 times and developed with the AP conjugate substrate kit (Bio-Rad Laboratories).

Immunofluorescence microscopy

Human MDA –MB-231 cells were fixed by 4% paraformadehyde. Fixed cells were washed with PBS 3 times and incubated in 1% Triton X-100 for 10 min. After 3 washing times with PBS, cells were blocked with 1% BSA in PBS for 1hr at room temperature. Then 1% BSA was removed and cells were incubated with purified goat anti-human Armet IgG (R&D Systems) and rabbit anti-58K Golgi protein IgG (Sigma-Aldrich) at 1:200 dilution in PBS with 5% non-fat dry milk overnight at 4 ℃. In the next morning, the first antibodies were removed. Then cells were washed with PBS 3 times and incubated with donkey anti-goat IgG (Alexa Fluor® 488, Invitrogen) and goat anti-rabbit IgG (Rhodamine Red^{TM}-X, Invitrogen) at 1:250 in PBS along with 1:5000 DAPI for 1 hr. After incubation, the secondary antibody and 4',6-diamidino-2-phenylindole (DAPI) were aspired and cells were washed 3 times with PBS. The coverslips were moved to filter papers and air dried before they were mounted with prolong antifade mounting solution. Photographs were taken using Leica DMI6000 B inverted microscope and analyzed by LAS AF (Leica application suite advanced fluorescence) software.

Circular dichroism (CD) spectroscopy

CD spectroscopy was performed with a Jasco 815 spectropolarimeter (Jasco, Tokyo, Japan) using a 0.1 cm path length cell over the 190-260 nm range. The spectra were acquired at room temperature every 1 nm with a 2 sec per data point and a 1 nm band pass. N-terminal 6X His-tagged human Armet was dissolved in 50 mM Tris-HCl, 100 mM NaCl, pH 7.0.

Differential scanning calorimetry (DSC) analysis

The effect of Ca^{2+} on thermal stability of human Armet in different buffer conditions was studied using a MicroCal VP-DSC calorimeter. Armet 1.5 mg/mL was dialyzed against 50 mM Tris-HCl, 100 mM NaCl, pH 7.0, 5 mM $CaCl_2 \cdot 2H_2O$; or against 50 mM Tris-HCl, 100 mM NaCl, pH 7.0, 2 mM EDTA. The dialysate buffers were placed in the reference cell during experiments. The cell pressure was set at 30 psi; the scan rate was set to 60 K/hr; and the scan range was 25-110 ℃. Prior to the scanning of protein samples, the baseline was checked using the dialysate buffers in both sample and reference cells. All scans were repeated four times on each protein sample. Data were analyzed using the "Origin for DSC"software.

Nuclear magnetic resonance (NMR) spectroscopy

NMR experiments were performed on a 500 MHz Varian NMR system spectrometer at 25 ℃. In calcium binding experiments, 2D ^{1}H-^{15}N HSQC spectra were acquired after addition of EDTA and $CaCl_2 \cdot 2H_2O$ to 0.3 mM ^{15}N labeled N-terminal 6X His-tagged human Armet in 50 mM Tris-HCl, pH 7.0. NMR data were analyzed by using MestReNova software.

Mass spectrometry

A protein solution was mixed with 3X volume of acetone in ice. After protein precipitate was collected and dissolved with 2% acetonitrile in 0.1 % trifluoroacetic acid solution. Then, 1.0 μL of the protein solution was dispensed along with 1.0 μL of 20 mg/mL DHB (Fluka/Sigma, St. Louis, MO) onto a stainless steel target plate. MALDI TOF spectra were acquired with a Bruker Ultraflex II (Bruker Daltonics) using Bruker protein molecular weight standard I (Bruker Daltonics) for molecular weight calibration.

Analytical ultracentrifuge (AUC)

Sedimentation velocity experiments were conducted using an Optima XL-I ultracentrifuge using the An-60 Ti rotor at 20 ℃. Protein samples were dialyzed against Tris buffer (50 mM Tris, 100 mM NaCl, pH 7.0); Tris buffer with 5 mM $CaCl_2 \cdot 2H_2O$; or Tris buffer with 5 mM DTT before apply to AUC experiments. Sedimentation was monitored at 280 nm using double sector cells with a sample volume of 400 μL per cell. Sedimentation was at 49,000 rpm with scans made at 5 min intervals. Sedimentation data were analyzed using DCDT+

software version 1.16 and sedimentation coefficients were calculated by using g(s*) fitting function in DCDT+ software.

Chapter 3 - Results

Immunofluorescence microscopy

Immunofluorescence microscopy was used to study the intracellular localization of Armet in human MDA-MB-231 cells. In Fig. 3.1, Armet was stained green and the Golgi was stained red. The staining of Armet was weaker in the periphery of cells and somewhat concentrated with the Golgi maker. It indicates Armet is localized in the Golgi and ER.

Expression and purification of human Armet

The N-terminal His-tagged fusion Armet was expressed in *E. coli* BL21 (DE3). High expression levels of recombinant protein were obtained after 1 mM IPTG induction (Fig. 3.2). His-tagged Armet was purified using a Ni^{2+}-affinity column. The purity was checked by SDS-PAGE (Fig. 3.2). With treatment of β-mercaptoethanol**,** one major band was observed with a molecular weight around 20 kDa. Without treatment with β-mercaptoethanol, two major bands with very similar migration distance were observed in the purified Armet, and a molecular ladder of higher molecular weight bands was observed**.**

In the cell lysate of induced *E.coli*, two bands with molecular masses close to 20 kDa were observed in SDS-PAGE and western blotting, but only in the absence of β-mercaptoethanol**.** Similar to the purified sample, a molecular ladder was also observed (Fig. 3.12, Fig. 3.13). The observations in the supernatant after sonication were consistent with the results of induced *E.coli* cells dissolved directly in the SDS sample buffer.

Ca2+-induced conformational changes of Armet

The CD spectrum of Armet did not change after EDTA was added (Fig. 9). CD spectra of Armet in several Ca^{2+} concentrations were collected. Armet exhibited spectral changes during the titration of Ca^{2+}. In the Ca^{2+} titration, conformational changes of Armet were detected at millimolar levels of Ca^{2+} (Fig. 3.4). Binding of Ca^{2+} by Armet was monitored by measuring negative molar ellipticity at 208 nm and 222 nm as a function of Ca^{2+} concentration. If we assume a single binding model, the dissociation constant would be in the millimolar range.

Thermal denaturation of Armet in the presence and absence of Ca2+

The first scan of Ca^{2+} free Armet showed one peak centered at 83 ℃. This corresponds to the melting temperature of the protein. The peak disappeared in the second scan (Fig. 3.5). This indicates that the unfolded Armet does not renature after heat denaturation. In the DSC spectrum of Ca^{2+} bound Armet, a smaller peak was observed, also centered at 83 ℃ (Fig. 3.5). This indicates the Tm of Armet did not change upon Ca^{2+} binding, but the protein was somewhat less structured.

Ca^{2+} binding examined by NMR

2D ^{1}H-^{15}N HSQC spectra were recorded for Armet in 50 mM Tris-HCl, pH 7.0 in the presence (8 mM) and absence of calcium (with 2 mM EDTA). Changes in chemical shift changes and signal intensity were observed (Fig. 3.6, Fig. 3.7, Fig. 3.8). After Ca^{2+} binding, chemical shift changes were observed in Gln18, Lys84, Lys114, and Glu132. Residues with increased signal strength included Gly55, His75, Ser134, Ser153, and Thr156. Residues with decreased signal strength included Asp5, Ile32, Ile37, Leu50, Asp58, Asp68, Ile76, Ile81, Tyr97, Ile101, Thr105, Ile135, Arg138, Asp157, and Leu158 (Fig. 3.9, Fig. 3.10). The observation suggested the binding of Ca^{2+} to Armet.

Molecular mass analysis by MALDI-TOF-MS

The mass of purified N-terminal His-tagged Armet was determined by matrix-assisted laser desorption/ionization (MALDI)-time-of-flight (TOF) mass spectrometry. Calculated molecular mass of the recombinant protein is 19,173 Da without the N-terminal Met. Masses obtained from the Ni-NTA purified protein sample were 19,038.808 Da (the main component), 19,136.514 Da, and 19,218.079 Da (Fig. 3.16).

SDS-PAGE without treatment of β-mercaptoethanol was used to separate two forms of Armet (Fig. 8). After electrophoresis, two bands with masses close to 20 kDa were cut out and analyzed by MALDI-TOF-MS. The detected mass of the lower band was 19048.74 Da, and the detected mass of the upper band was 19054.011 Da (Fig. 3.15). The result suggested the different migration properties of these two bands on SDS-PAGE were not caused by different masses.

Ultracentrifugation

Sedimentation velocity at different buffer conditions was performed. In the purified protein sample, one peak was observed at 2 S and a smear was observed around 4 S. This suggested that most protein was in the monomer form, and a small portion of protein was in the oligomer form. No change was observed after Ca^{2+} was added. With 5 mM DTT, the smear around 4 S disappeared when the peak at 2 S increased (Fig. 3.17). From the plot of log(sedimentation constant) against log(molecular weight) (Halsall et al., 1982), sedimentation constant for Armet as a monomer (19,173 Da) is around 2.4, which is close to observed sedimentation coefficient of about 2 S.

Chapter 4 - Discussion and Conclusions

Intracellular localization of human Armet

Armet, a secreted protein, is expected to occur in the ER. And some evidence indicates Armet is, to some extent, retained in the ER. A C-terminal ER retention signal, RTDL, is conserved in amphibian and mammal Armet, and other KDEL-like sequences are also are found in insect Armet.

Secreted Armet was first found in a rat mesencephalic type-1 astroycte cell line culture medium as a neurotrophic factor (Petrova et al., 2003). In an immunofluorescence study, Armet was colocalized with ER resident protein disulfide isomerase in Balb/c 3T3 cells and was easily extracted from microsomes in alkaline extraction. This indicated Armet was an ER protein that was not bound to the membrane (Mizobuchi et al., 2007). Apostolu et al. (2008) showed in Hela cells transfected with ER protein Hrd1that Armet was found colocalized with Hrd1 and Golgin-97, a Golgi marker by immunofluorescence staining.

In a study of different C-terminal KDEL-like motifs, Raykhel et al. (2007) found C-terminal RTDL resulted in the efficient ER localization of a reporter construct with an N-terminal secretion signal. Immunofluorescence localization of the protein encoded by this construct was mainly found in the ER and little was found in the Golgi (Raykhel et al., 2007).

In this work, double immunofluorescent staining of Armet and a Golgi in human breast cancer MBA-MD-231 cells was performed. The staining of endogenous Armet was weaker in the periphery of the cells than near the nucleus where it colocalized with the Golgi maker. This indicated Armet was localized in the Golgi and presumably also in the ER. Our result, combined with other groups' observations, suggests that Armet is found in ER not only because it is a secreted protein, but also because it is retained in the ER. Armet's localization indicates its potential function in the ER during ER stress.

Ca2+ binding of human Armet

Previously in our lab, Dr. Feng Cui found that Armet from pea aphid was a calcium binding protein. In this study, several biophysical techniques were used to explore a possible interaction between human Armet and calcium ion. The CD spectrum of purified Armet protein

showed negative peaks at 208 nm and 222 nm, which indicated a characteristic α-helix. In the presence of Ca^{2+}, the ellipticity at 208 and 222 nm decreased. This suggests a structural change due to helix-helix interactions (Mani et al., 1982, Santamaria-Kisiel et al., 2011). The free Ca^{2+} concentration in the ER intraluminal space varies from 0.2-1 mM (Verkhratsky et al., 2003). Some ER proteins are Ca^{2+}-binding proteins such as calreticulin and calnexin (Michalak et al., 2002). Their calcium binding affinity is mostly in micromolar range. K_D values of a common calcium binding motif, EF hand, are in micromolar range as well (Hebenstreit et. al, 2005). Calcium binding by an ER protein with low affinity and high capacity is also reported. For example, calreticulin can bind calcium with K_D values of 17 μM and 0.6 mM (Wijeyesakere et al., 2010).

The DSC results seem consistent with the CD results. Without Ca^{2+}, one peak was observed, centered at 85℃. With 5 mM Ca^{2+}, a smaller peak was detected at the same temperature. This indicated the melting temperature of Armet did not change upon Ca^{2+}-binding, but less structure existed in the protein with calcium bound.

In sedimentation velocity experiments, Ca^{2+} did not increase the content of oligomers formed in purified Armet sample. This indicated that Ca^{2+} induced protein conformational change that did not affect interaction between Armet molecules.

In 2D ^{1}H-^{15}N HSQC spectra of Armet, peak intensity changes and perturbation of peak chemical shifts verified the binding between Armet and Ca^{2+}. Around 30 of the 120 detected peaks were significantly changed after Ca^{2+} was added. The residues losing intensity of HSQC crosspeaks had reduced mobility upon Ca^{2+} binding. Perturbations of residue chemical shifts indicated the change of chemical environment around these affected residues. From sequence alignment (Fig. A.7), negatively charged residues (Asp5, Asp121, Glu132, Asp135, Asp157) perturbed upon calcium binding are conserved. Although no traditional calcium binding motif exists in Armet, affected amino acid residues Glu132 and Asp135 could form part of a cluster of negatively charged side chains that could possibly form a binding site for a calcium ion. Due to flexibility of the linker region of Armet, it is also possible that Asp157 at the C-terminus could interact with other residues with negatively charged side chains to form another calcium binding site.

Heterogeneity of human Armet

Eight conserved cysteines were found in all Armets. Four cysteines participate in two CXXC motifs. CXXC motifs occur in disulfide isomerases and may indicate similar function in Armet (Parkash et al., 2010). But the α-helix rich structure of Armet is very different from the thioredoxin fold (an α/β structure) (N. Mizobuchi et al., 2007). A heterogeneity of disulfide bonds in mouse Armet was described in previous publications, but not discussed. Using MALDI-TOF MS, Mizobuchi et al. (2007) identified three intramolecular disulfide bonds at Cys6-Cys9, Cys 40-Cys51, and Cys 127-130. In another MALDI-TOF MS study, Hoseki et al. (2010) suggested disulfide bonds at Cys6-Cys93/Cys9-Cys93, Cys6-Cys82/Cys9-Cys82, Cys40-Cys51, and Cys127-Cys130 (Table 4.1).

No disulfide bond heterogeneity in human Armet has been reported. In this study, two bands of slightly different mobility were observed in SDS gels run in the absence of reducing agent on purified Armet. Molecular weight analysis by MALDI-TOF MS showed these two bands had masses of 19048.74 Da and 19054.011 Da. Thus the mobility difference for the two bands is not due to differences in mass. I suggest that mobility difference might due to alternate disulfide bonds arrangement. Also, without any reducing reagent, a faint ladder was formed by Armet in SDS gels and westenblottings. The calculated masses of bands in the ladder are 38 and 60 kDa from westernblotting (Fig. 3.13). This indicates about 12% (calculated form SDS gels) purified Armet formed oligomers. Disappearance of the ladder in the presence of reducing agent indicated formation of disulfides between Armet molecules. Sedimentation velocity experiments also suggested a portion of Armet formed oligomers though intermolecular disulfide bonds in 50 mM Tris-HCl, 100 mM NaCl, pH 7.0. These results indicate existence of free cysteines in Armet's expression in *E.coli*. In the study of human Armet's crystal structure, the protein was crystallized as monomer at 4℃ in 100 mM Na-cacodylate buffer, pH 6.5, 0.2 M MgAc2 and 12–18% (w/v) PEG 8000 (Parkash et al., 2010). The monomer observed in crystal structure might be explained as effect of temperature. Whether Armet can form oligomeres in mammalian cells needs to be studied.

Finally, minor species of mass differences of 98 and 180 with respect to the main protein component were observed by MALDI-TOF MS. Perhaps this can be explained by phosphorylation modification of some amino acid residues.

Conclusions and future work

Results from CD and NMR indicate that human Armet is a calcium binding protein. Calcium binding could cause conformational change and loss of CD signal in the protein. DSC results indicated Armet was less structured upon calcium binding. The next logical step is to make mutants to verify those hypothetical binding sites. Negatively charged residues (Asp5, Asp 121, Glu 132, Asp 135 and Asp157) with perturbed crosspeaks in NMR experiments might form calcium binding sites. It is interesting to test whether mutants in these positions will affect Armet's calcium binding property. These negatively residues can either be alternated by neutral Asn or Gln residues or to the small Gly residue. Mutations could also be made in the linker region because its flexibility might be involved in ligand binding of Armet. Within residues in the linker region, Lys114's crosspeak showed the most significant change in the HSQC spectrum upon calcium binding of Armet. An experiment could be done with Lys114-Pro114 mutant to reduce flexibility of the linker region.

Three types of heterogeneity of Armet were found in this study. In recombinant *E.coli* cells and extract, two Armet species were detected with possible different disulfide bond arrangements. A ladder formed by Armet linked with intermolecular disulfide bonds was observed. And mass heterogeneity of Armet was also detected. Whether two species of Armet and the ladder exist in human cell needs to be studied by westernblotting with and without ER stress.

Figure 1.1 Alignment of Armet from vertebrates and invertebrates.

Residues highlighted in yellow are cysteines. C-terminal ER retention signals are highlighted in Pink. The stars, dots and colons below the alignment sequences indicate the level of similarity at each position.

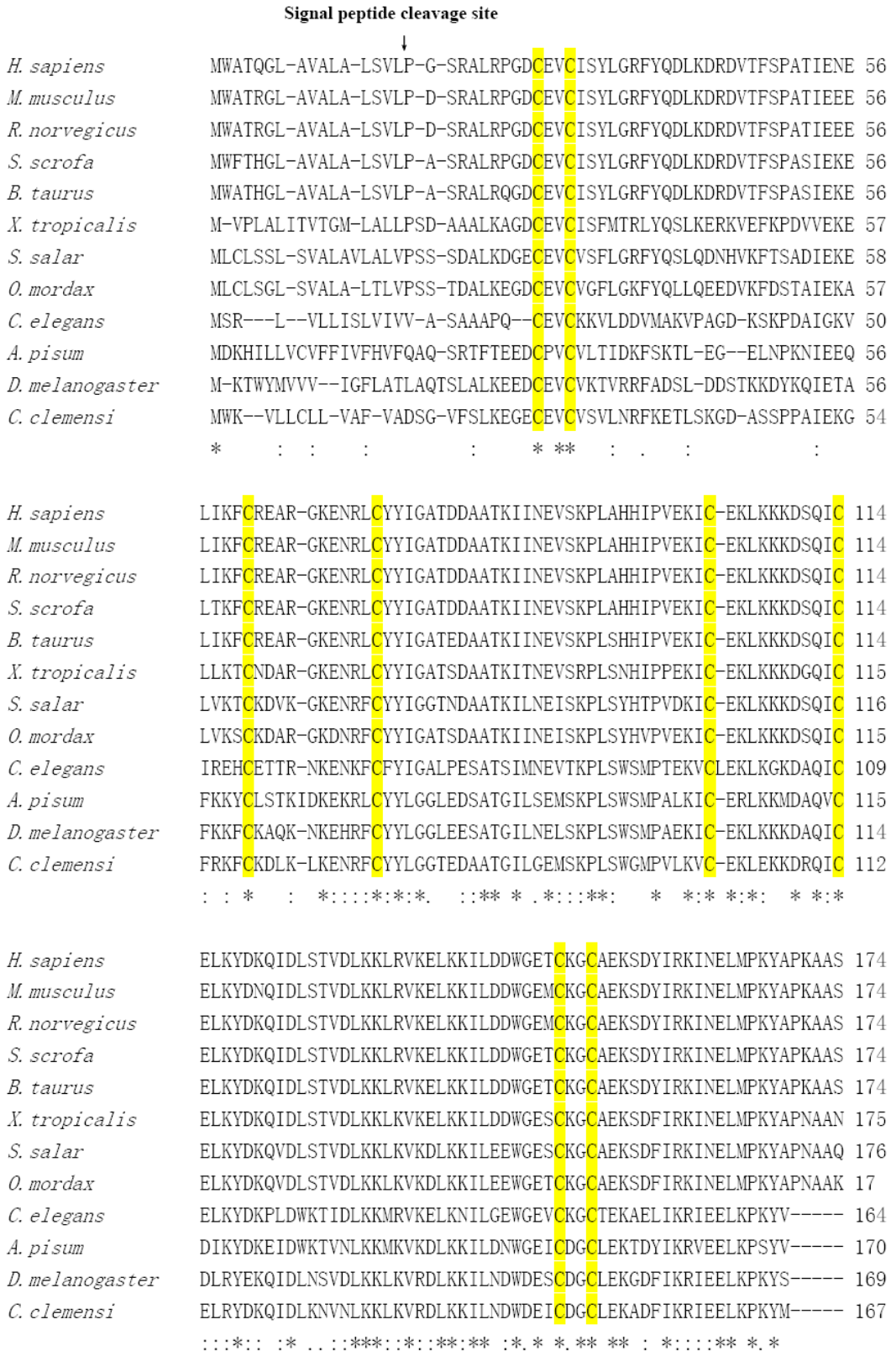
Signal peptide cleavage site
H. sapiens MWATQGL-AVALA-LSVLP-G-SRALRPGDCEVCISYLGRFYQDLKDRDVTFSPATIENE 56
M. musculus MWATRGL-AVALA-LSVLP-D-SRALRPGDCEVCISYLGRFYQDLKDRDVTFSPATIEEE 56
R. norvegicus MWATRGL-AVALA-LSVLP-D-SRALRPGDCEVCISYLGRFYQDLKDRDVTFSPATIEEE 56
S. scrofa MWFTHGL-AVALA-LSVLP-A-SRALRPGDCEVCISYLGRFYQDLKDRDVTFSPASIEKE 56
B. taurus MWATHGL-AVALA-LSVLP-A-SRALRQGDCEVCISYLGRFYQDLKDRDVTFSPASIEKE 56
X. tropicalis M-VPLALITVTGM-LALLPSD-AAALKAGDCEVCISFMTRLYQSLKERKVEFKPDVVEKE 57
S. salar MLCLSSL-SVALAVLALVPSS-SDALKDGECEVCVSFLGRFYQSLQDNHVKFTSADIEKE 58
O. mordax MLCLSGL-SVALA-LTLVPSS-TDALKEGDCEVCVGFLGKFYQLLQEEDVKFDSTAIEKA 57
C. elegans MSR---L--VLLISLVIVV-A-SAAAPQ--CEVCKKVLDDVMAKVPAGD-KSKPDAIGKV 50
A. pisum MDKHILLVCVFFIVFHVFQAQ-SRTFTEEDCPVCVLTIDKFSKTL-EG--ELNPKNIEEQ 56
D. melanogaster M-KTWYMVVV--IGFLATLAQTSLALKEEDCEVCVKTVRRFADSL-DDSTKKDYKQIETA 56
C. clemensi MWK--VLLCLL-VAF-VADSG-VFSLKEGECEVCVSVLNRFKETLSKGD-ASSPPAIEKG 54
H. sapiens LIKFCREAR-GKENRLCYYIGATDDAATKIINEVSKPLAHHIPVEKIC-EKLKKKDSQIC 114
M. musculus LIKFCREAR-GKENRLCYYIGATDDAATKIINEVSKPLAHHIPVEKIC-EKLKKKDSQIC 114
R. norvegicus LIKFCREAR-GKENRLCYYIGATDDAATKIINEVSKPLAHHIPVEKIC-EKLKKKDSQIC 114
S. scrofa LTKFCREAR-GKENRLCYYIGATDDAATKIINEVSKPLAHHIPVEKIC-EKLKKKDSQIC 114
B. taurus LIKFCREAR-GKENRLCYYIGATEDAATKIINEVSKPLSHHIPVEKIC-EKLKKKDSQIC 114
X. tropicalis LLKTCNDAR-GKENRLCYYIGATSDAATKITNEVSRPLSNHIPPEKIC-EKLKKKDGQIC 115
S. salar LVKTCKDVK-GKENRFCYYIGGTNDAATKILNEISKPLSYHTPVDKIC-EKLKKKDSQIC 116
O. mordax LVKSCKDAR-GKDNRFCYYIGATSDAATKIINEISKPLSYHVPVEKIC-EKLKKKDSQIC 115
C. elegans IREHCETTR-NKENKFCFYIGALPESATSIMNEVTKPLSWSMPTEKVCLEKLKGKDAQIC 109
A. pisum FKKYCLSTKIDKEKRLCYYLGGLEDSATGILSEMSKPLSWSMPALKIC-ERLKKMDAQVC 115
D. melanogaster FKKFCKAQK-NKEHRFCYYLGGLEESATGILNELSKPLSWSMPAEKIC-EKLKKKDAQIC 114
C. clemensi FRKFCKDLK-LKENRFCYYLGGTEDAATGILGEMSKPLSWGMPVLKVC-EKLEKKDRQIC 112
H. sapiens ELKYDKQIDLSTVDLKKLRVKELKKILDDWGETCKGCAEKSDYIRKINELMPKYAPKAAS 174
M. musculus ELKYDNQIDLSTVDLKKLRVKELKKILDDWGEMCKGCAEKSDYIRKINELMPKYAPKAAS 174
R. norvegicus ELKYDKQIDLSTVDLKKLRVKELKKILDDWGEMCKGCAEKSDYIRKINELMPKYAPKAAS 174
S. scrofa ELKYDKQIDLSTVDLKKLRVKELKKILDDWGETCKGCAEKSDYIRKINELMPKYAPKAAS 174
B. taurus ELKYDKQIDLSTVDLKKLRVKELKKILDDWGETCKGCAEKSDYIRKINELMPKYAPKAAS 174
X. tropicalis ELKYDKQIDLSTVDLKKLKVKELKKILDDWGESCKGCAEKSDFIRKINELMPKYAPNAAN 175
S. salar ELKYDKQVDLSTVDLKKLKVKDLKKILEEWGESCKGCAEKSDFIRKINELMPKYAPNAAQ 176
O. mordax ELKYDKQVDLSTVDLKKLKVKDLKKILEEWGETCKGCAEKSDFIRKINELMPKYAPNAAK 17
C. elegans ELKYDKPLDWKTIDLKKMRVKELKNILGEWGEVCKGCTEKAELIKRIEELKPKYV----- 164
A. pisum DIKYDKEIDWKTVNLKKMKVKDLKKILDNWGEICDGCLEKTDYIKRVEELKPSYV----- 170
D. melanogaster DLRYEKQIDLNSVDLKKLKVRDLKKILNDWDESCDGCLEKGDFIKRIEELKPKYS----- 169
C. clemensi ELRYDKQIDLKNVNLKKLKVRDLKKILNDWDEICDGCLEKADFIKRIEELKPKYM----- 167

H. sapiens	ARTDL	179
M. musculus	ARTDL	179
R. norvegicus	ARTDL	179
S. scrofa	SRTDL	179
B. taurus	SRTDL	179
X. tropicalis	ARTDL	180
S. salar	ARTDL	181
O. mordax	ARTEL	180
C. elegans	-KEEL	168
A. pisum	-KEEL	174
D. melanogaster	-RSEL	173
C. clemensi	-REGL	171
	: *	

Figure 1.2 Alignment of full-length human and mouse Armets.

N-terminal signal peptides are colored in blue. Residues highlighted in yellow are cysteines. Residues that are different in human and mouse Armets are highlighted in gray. C-terminal ER retention signals are highlighted in Pink.

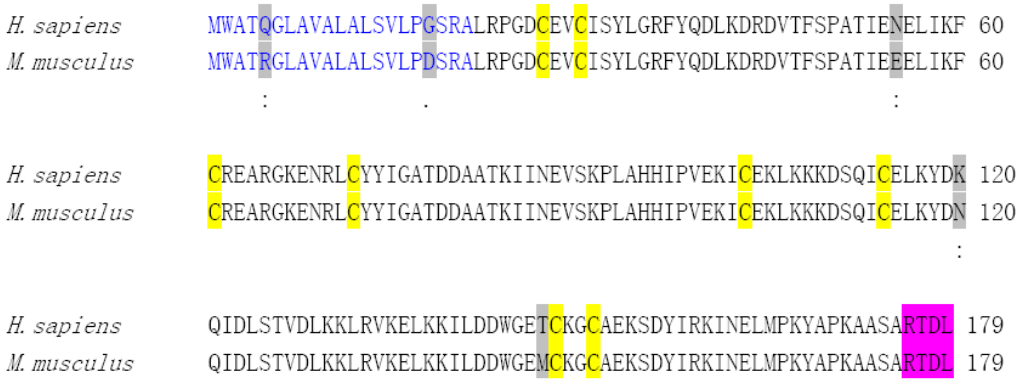
H. sapiens MWATQGLAVALALSVLPGSRALRPGDCEVCISYLGRFYQDLKDRDVTFSPATIENELIKF 60
M. musculus MWATRGLAVALALSVLPDSRALRPGDCEVCISYLGRFYQDLKDRDVTFSPATIEEELIKF 60
H. sapiens CREARGKENRLCYYIGATDDAATKIINEVSKPLAHHIPVEKICEKLKKKDSQICELKYDK 120
M. musculus CREARGKENRLCYYIGATDDAATKIINEVSKPLAHHIPVEKICEKLKKKDSQICELKYDN 120
H. sapiens QIDLSTVDLKKLRVKELKKILDDWGETCKGCAEKSDYIRKINELMPKYAPKAASARTDL 179
M. musculus QIDLSTVDLKKLRVKELKKILDDWGEMCKGCAEKSDYIRKINELMPKYAPKAASARTDL 179

Figure 1.3 Recombinant plasmid and sequence of N-terminal 6X His-tagged mature human Armet expressed in *E.coli*.

Sequence of mature human Armet was cloned in pET-28a(+) plasmid between NcoI and XhoI restriction enzyme cleavage sites (highlighted in blue in the plasmid map). Six-histidine tag is highlighted in blue, eight cysteines are highlighted in yellow, and the C-terminal ER retention signal is highlighted in pink.

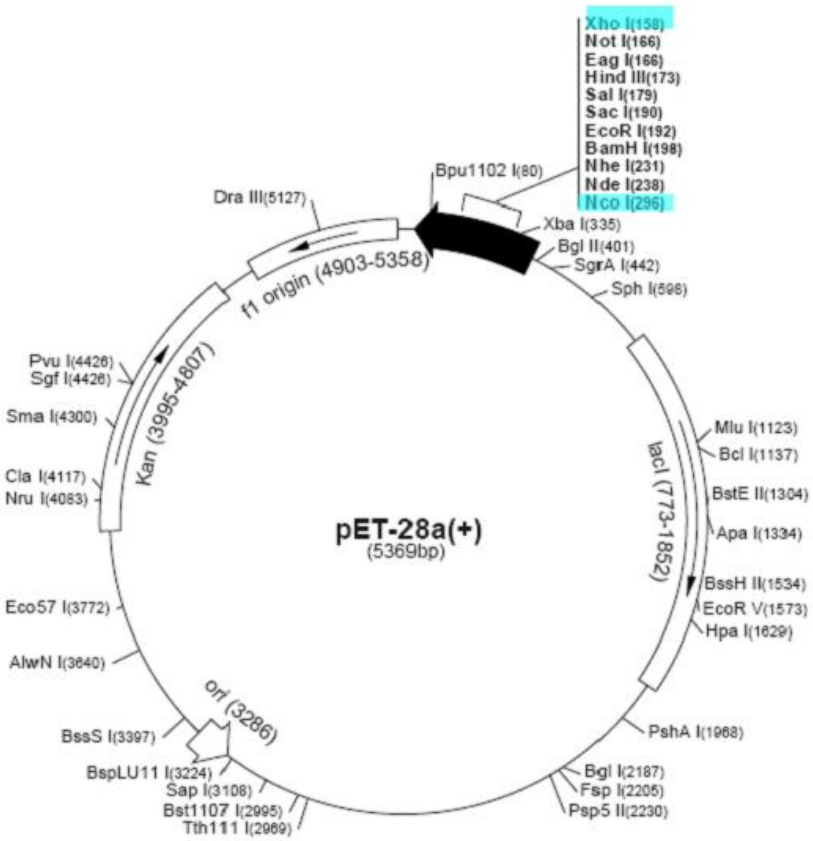

M G H H H H H H L R P G D C E V C I S Y L G R F Y Q D L K D R D V T F S P A T I E N
E L I K F C R E A R G K E N R L C Y Y I G A T D D A A T K I I N E V S K P L A H H I
P V E K I C E K L K K K D S Q I C E L K Y D K Q I D L S T V D L K K L R V K E L K K
I L D D W G E T C K G C A E K S D Y I R K I N E L M P K Y A P K A A S A R T D L

Figure 1.4 Crystal structure of human Armet (residue 1 to 137) (Parkash et al., 2009).

Helices are shown as cylindrical structure. Side chains of conserved cysteines are colored blue.

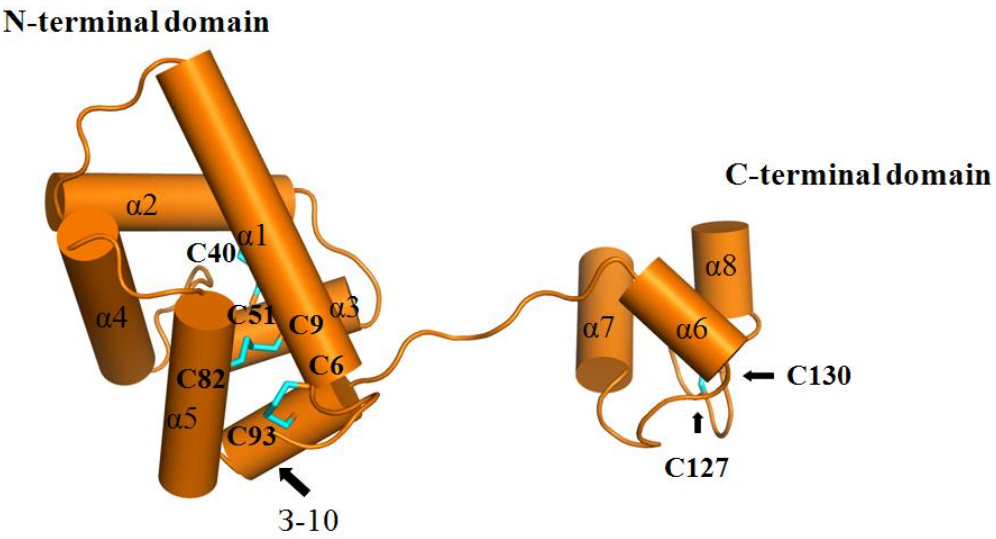
N-terminal domain
C-terminal domain
α2
α1
C40
α4
C51
C9
α3
C82
C6
α5
C93
3-10
α7
α8
α6
C130
C127

Figure 1.5 Three dimensional structures of human and mouse Armet.

(1) Crystal structure of human Armet (Parkash et al., 2009).

(2) NMR structure of human Armet (Hellman et al., 2010).

(3) NMR structure of mouse Armet (Hoseki et al., 2010).

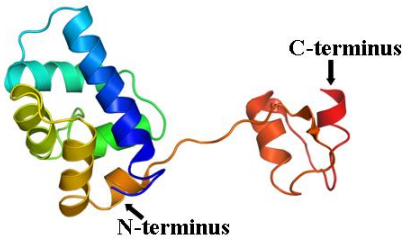
C-terminus
N-terminus

1

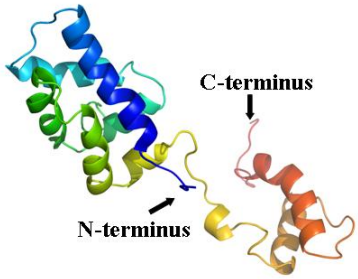
C-terminus
N-terminus

2

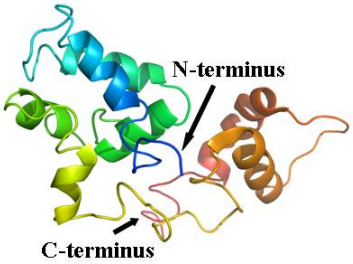
N-terminus
C-terminus

3

Figure 1.6 Structural superimposition of Armets.

(1) Superimposition of NMR and crystal structures of human Armet (NMR structure is gold and crystal structure is blue).

(2) Superimposition of NMR structures of human and mouse Armet (Human Armet structure is gold and mouse Armet structure is green).

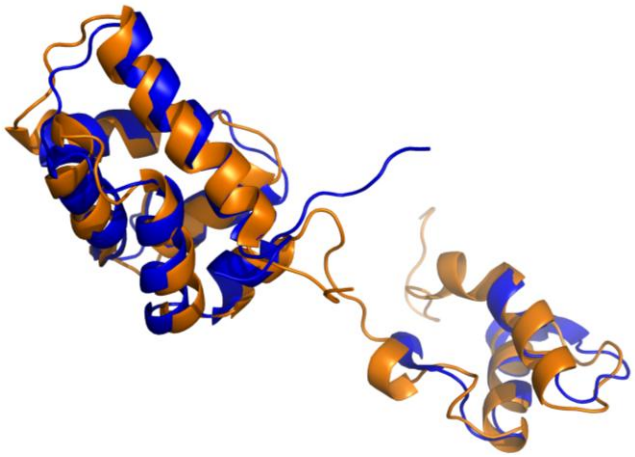

1

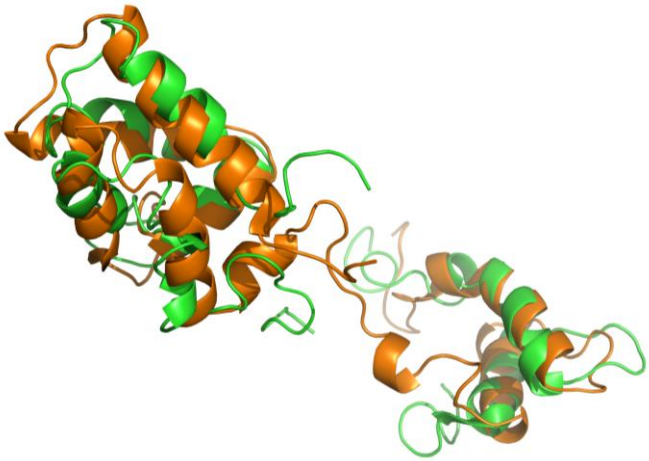

2

Figure 3.1 Armet localization in human MDA-MB-231 cells.

(1) Immunofluorescence staining of Armet using goat anti-human Armet human antibodies and donkey-anti goat IgG.

(2) Immunofluorescence staining of Golgi using rabbit anti-58K Golgi protein antibodies and goat anti rabbit IgG.

(3) Overlay of Armet (green) and Golgin-97 (red) stained images.

(4) Immunofluorescence staining of Armet, Golgi, and nuclei. Nuclei were stained in blue using DAPI.

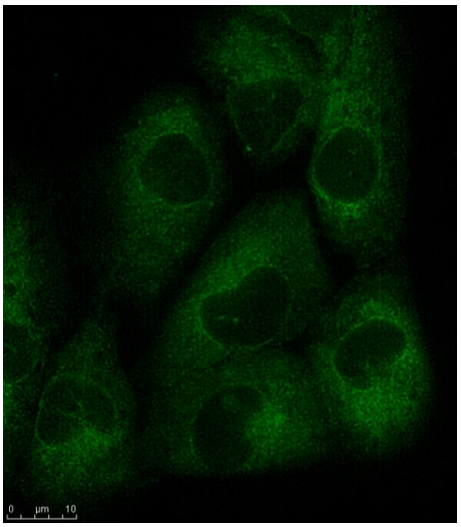

1

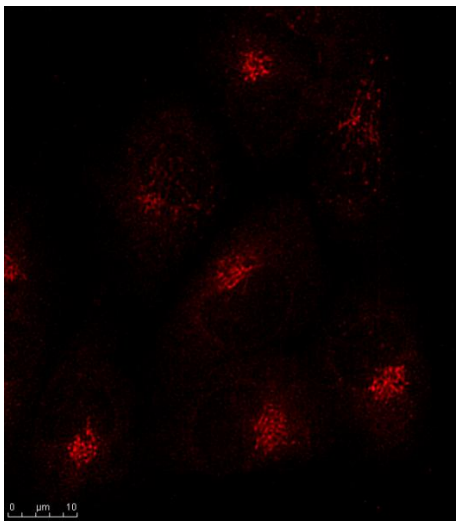

2

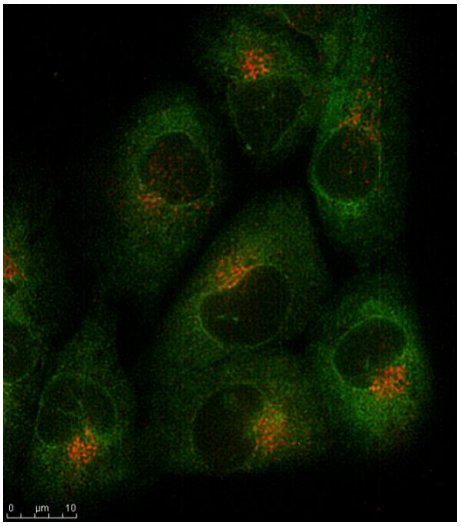

3

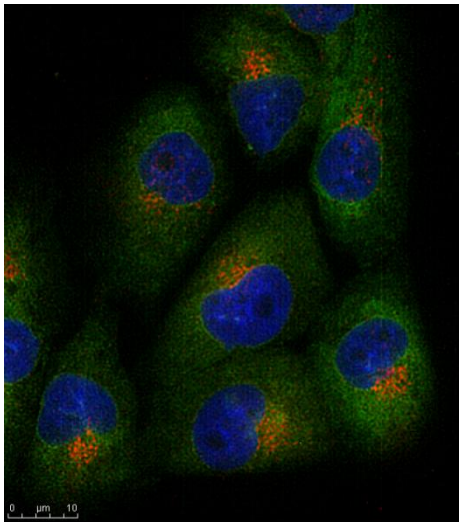

4

Figure 3.2 SDS gel electrophoresis of samples from N-terminal 6X His-tagged human Armet expressed in *E. coli* and purified by Ni-NTA.

Lane 1: molecular mass ladders.

Lane 2: *E. coli* cells without IPTG induction.

Lane 3: *E. coli* cells with 1mM IPTG induction.

Lane 4: Induced *E. coli* supernatant after sonication.

Lane 5: Flowthrough from Ni-NTA column.

Lane 6: Purified protein in 50 mM Tris-HCl, 100 mM NaCl, pH 7.0.

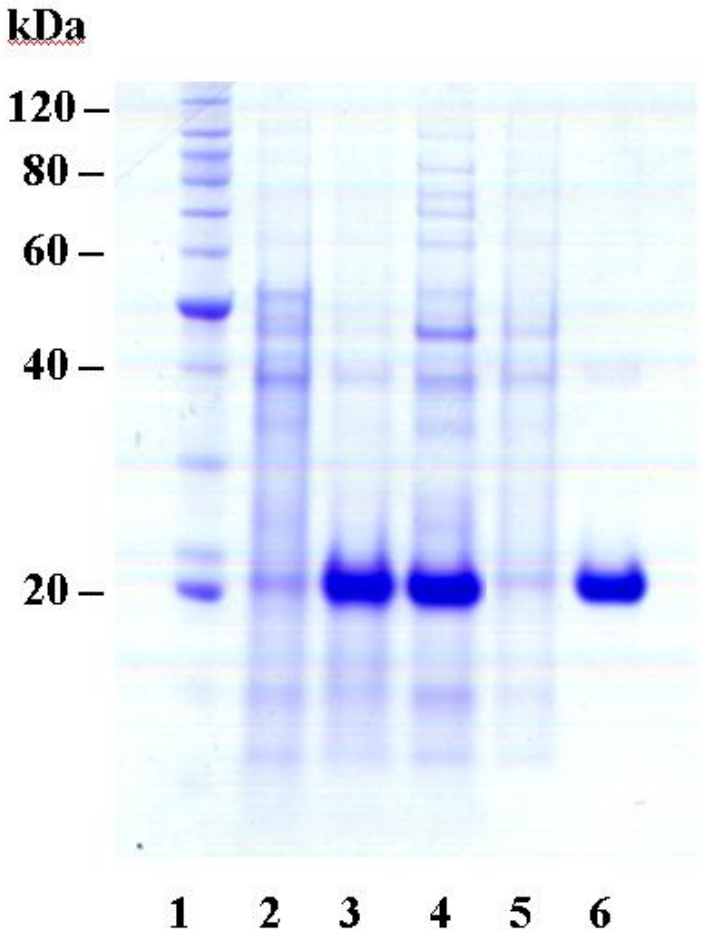
kDa
120 –
80 –
60 –
40 –
20 –
1
2
3
4
5
6

Figure 3.3 Far UV CD spectra of Armet in the presence and absence of EDTA

Armet sample was prepared in 50 mM Tris, 100 mM NaCl, pH 7.0. Protein concentration was 0.03 mM. EDTA concentration was 1 mM.

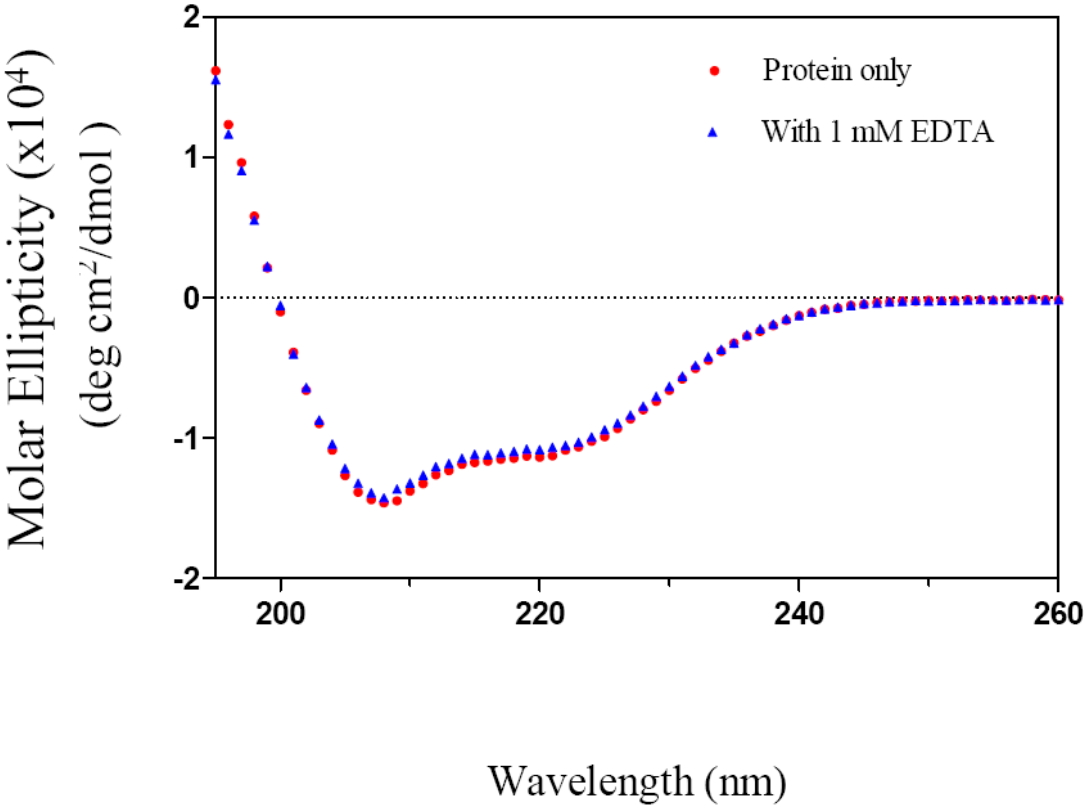
Molar Ellipticity (x10⁴)
(deg cm²/dmol)
2
1
0
-1
-2
200
220
240
260
Protein only
With 1 mM EDTA
Wavelength (nm)

Figure 3.4 Far UV CD spectra of Armet in the presence of EDTA and Ca^{2+}.

Armet samples were prepared in 50 mM Tris-HCl, 100 mM NaCl, pH 7.0. Protein concentrations were 0.013 mM (1) and 0.0166 mM (2).

(1) and (2) are two independent experiments.

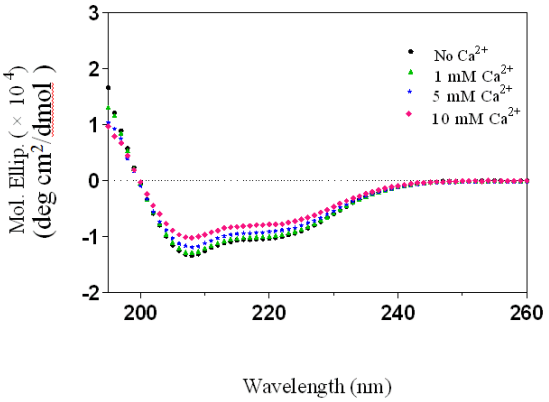

Jan 10th. 2011

1

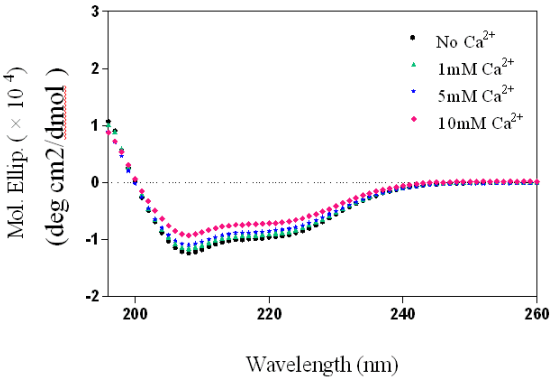

Jan 20th. 2011

2

Figure 3.5 Differential scanning calorimetry of Armet in the presence of EDTA and Ca^{2+}. Armet samples were prepared in 50 mM Tris-HCl, 100 mM NaCl, pH 7.0. Protein concentration was 0.04 mM.

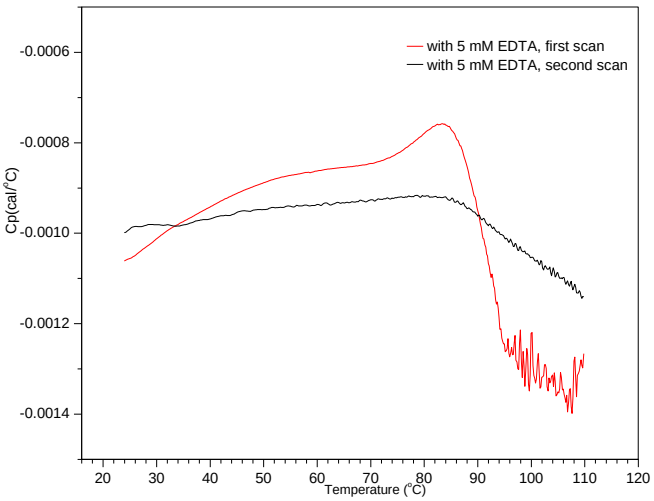
with 5 mM EDTA, first scan
with 5 mM EDTA, second scan
Cp(cal/°C)
-0.0006
-0.0008
-0.0010
-0.0012
-0.0014
20
30
40
50
60
70
80
90
100
110
120
Temperature (°C)

1

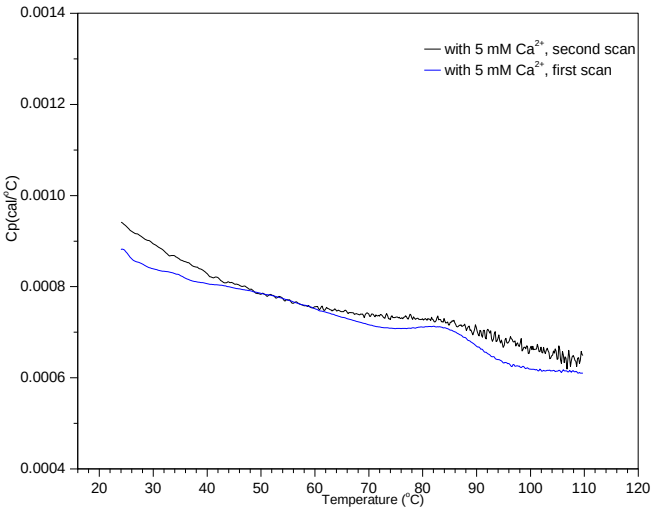
with 5 mM Ca2+, second scan
with 5 mM Ca2+, first scan
Cp(cal/°C)
0.0014
0.0012
0.0010
0.0008
0.0006
0.0004
20
30
40
50
60
70
80
90
100
110
120
Temperature (°C)

2

Figure 3.6 2D ^{1}H-^{15}N HSQC spectrum of Armet.

Buffer: 50 mM Tris-HCl, 2 mM EDTA, pH 7.0. Protein concentration was 0.23 mM. Spectrum was recorded at 35 ℃.

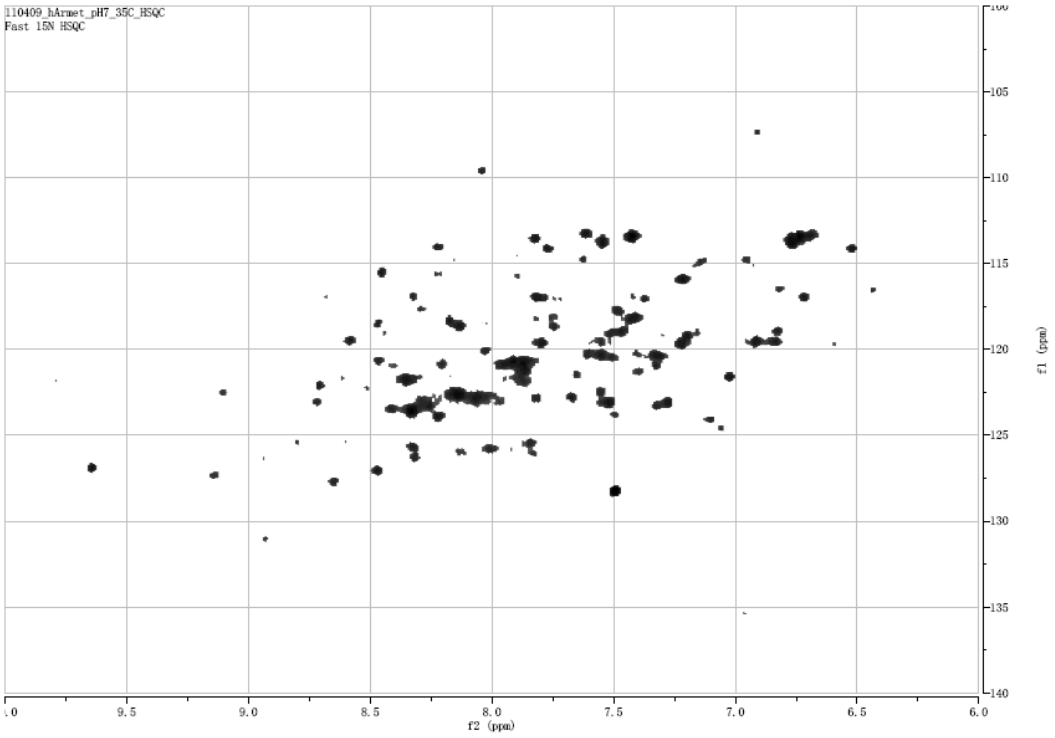
110409_hArnet_pH7_35C_HSQC
Fast 15N HSQC
105
110
115
120
125
130
135
140
f1 (ppm)
9.5
9.0
8.5
8.0
7.5
7.0
6.5
6.0
f2 (ppm)

Figure 3.7 2D ^{1}H-^{15}N HSQC spectrum of Ca^{2+}-bound Armet.

Buffer: 50 mM Tris-HCl, 2 mM EDTA, 10 mM $CaCl_2$, pH 7.0. Protein concentration was 0.3 mM. Spectrum was recorded at 35 ℃.

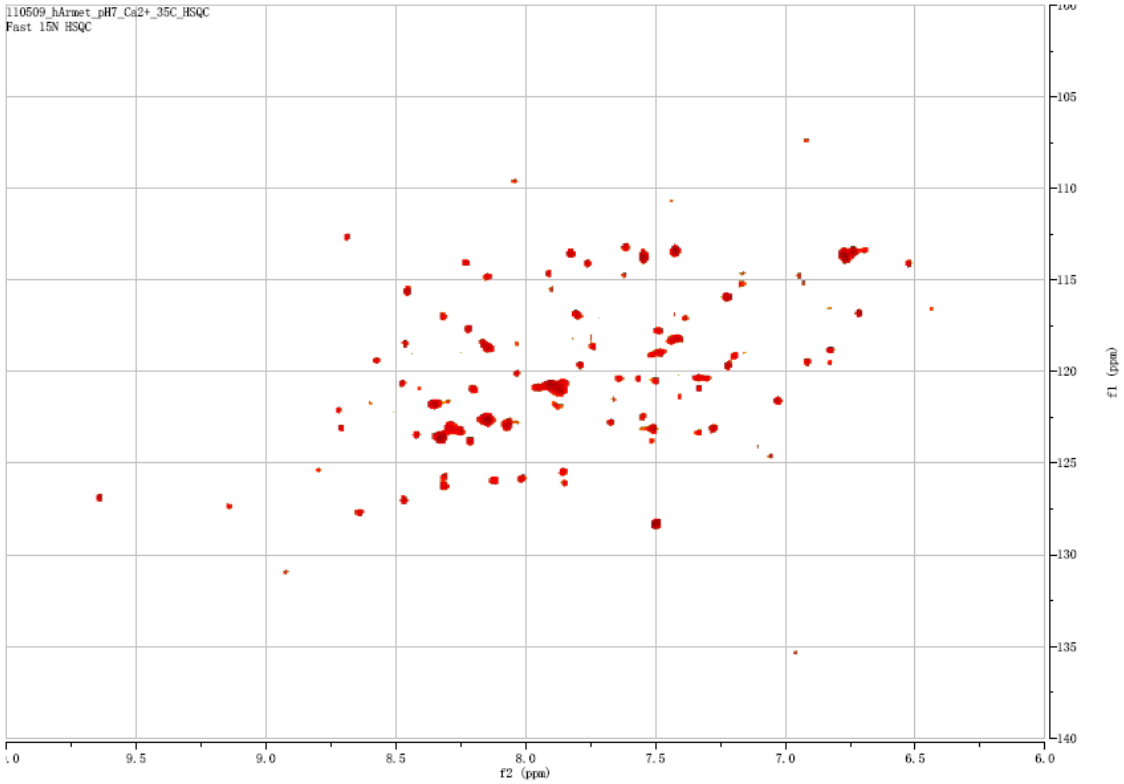
110509_hArmet_pH7_Ca2+_35C_HSQC
Fast 15N HSQC
105
110
115
120
125
130
135
140
f1 (ppm)
9.5
9.0
8.5
8.0
7.5
7.0
6.5
6.0
f2 (ppm)

Figure 3.8 Overlaid 2D ^{1}H-^{15}N HSQC spectra of Armet in the absence and in the presence of Ca^{2+}.

Black: Armet without Ca^{2+}.

Red: Armet with Ca^{2+}.

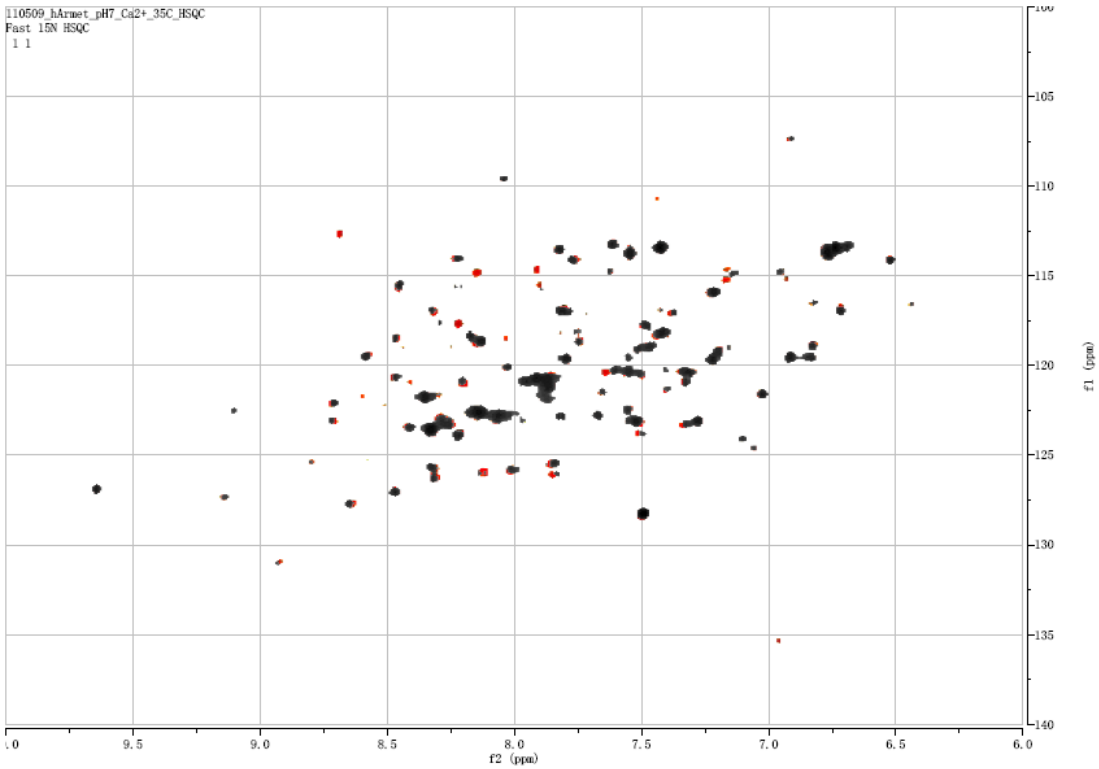
110509_hArmet_pH7_Ca2+_35C_HSQC
Fast 15N HSQC
1 1
105
110
115
120
125
130
135
140
f1 (ppm)
9.5
9.0
8.5
8.0
7.5
7.0
6.5
6.0
f2 (ppm)

Figure 3.9 2D ^{1}H-^{15}N HSQC difference spectrum of Armet.

Blue: Peaks with decreased signal strength in the presence of Ca^{2+}.

Red: Peaks with increased signal strength in the presence of Ca^{2+}.

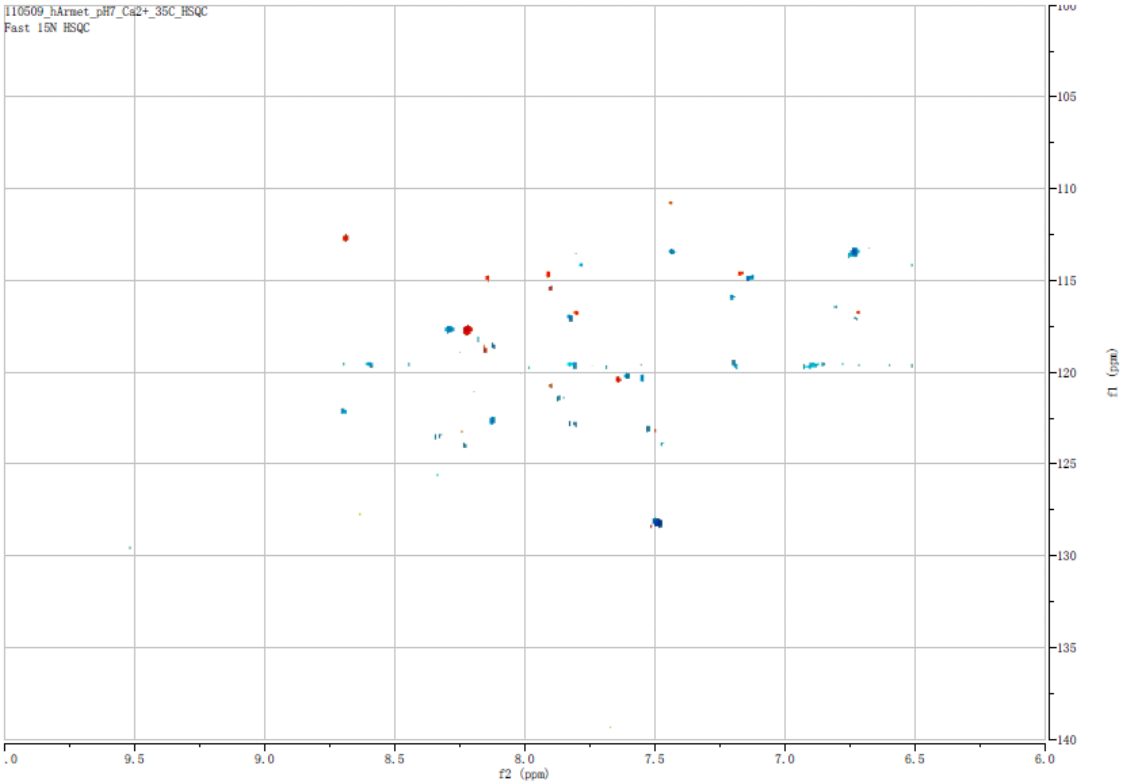
110509_hArmet_pH7_Ca2+_35C_HSQC
Fast 15N HSQC
105
110
115
120
125
130
135
140
f1 (ppm)
.0
9.5
9.0
8.5
8.0
7.5
7.0
6.5
6.0
f2 (ppm)

Figure 3.10 2D ^{1}H-^{15}N HSQC difference spectrum of Armet.

Residues with significant changes are labeled using HSQC spectrum in previous human Armet NMR study (Hellman et al., 2010).

Blue: Peaks with decreased signal strength in the presence of Ca^{2+}.

Red: Peaks with increased signal strength in the presence of Ca^{2+}.

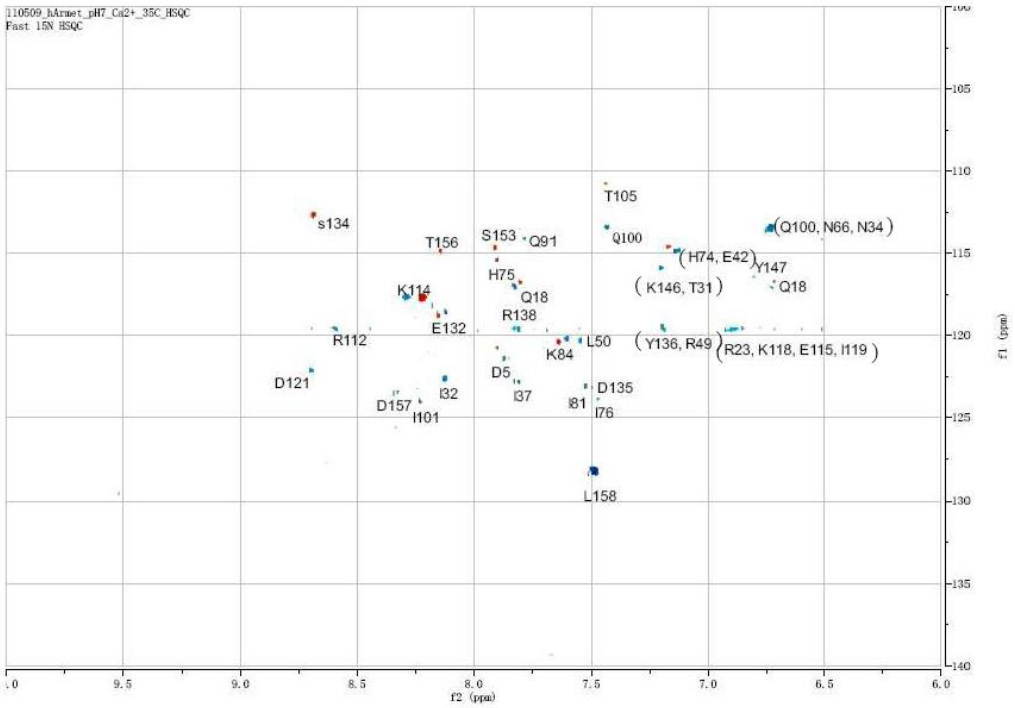
110509_hArmet_pH7_Ca2+_35C_HSQC
Fast 15N HSQC
T105
s134
(Q100, N66, N34)
T156
S153
Q91
Q100
(H74, E42)
Y147
H75
(K146, T31)
Q18
K114
Q18
R138
E132
R112
L50
(Y136, R49)
(R23, K118, E115, I119)
K84
D5
D121
D135
I32
I37
I81
D157
I76
I101
L158
f2 (ppm)
f1 (ppm)

Figure 3.11 Residues in Armet with changed 2D ^{1}H-^{15}N HSQC signals in the presence of Ca^{2+}.

(1) and (2): Perturbed glutamic acid and aspartic acid residues were colored in blue.

(3) and (4): Perturbed amino residues in Ca^{2+}-bound Armet. Residues with perturbed chemical shifts were colored in green, residues with increased signal were colored in pink, and residues with decreased signal were colored in blue.

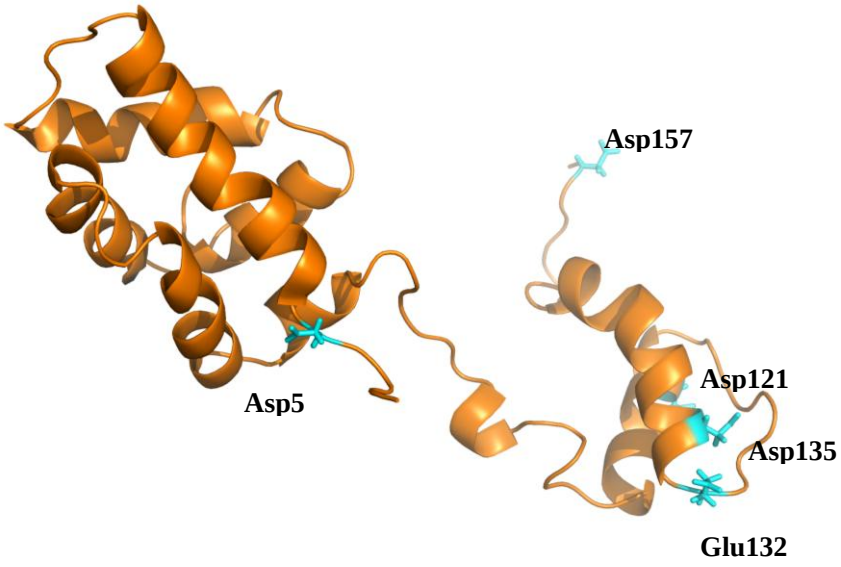
Asp157
Asp121
Asp135
Asp5
Glu132

1

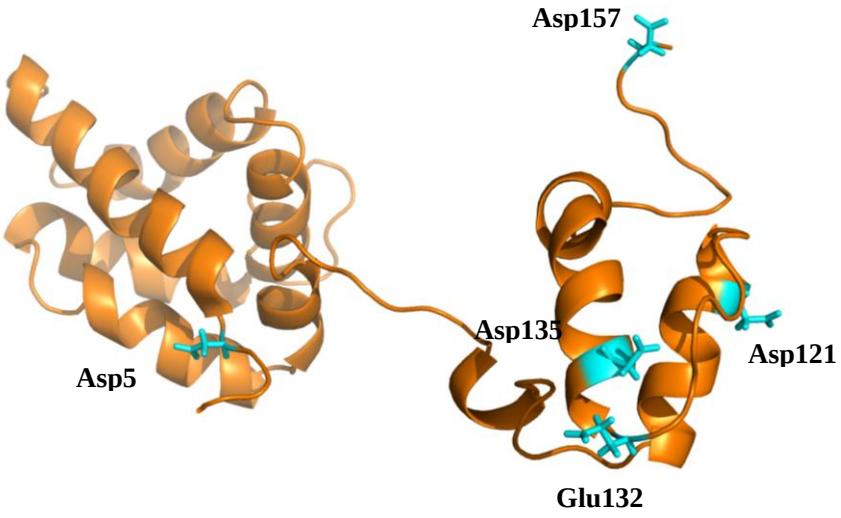
Asp157
Asp135
Asp121
Asp5
Glu132

2

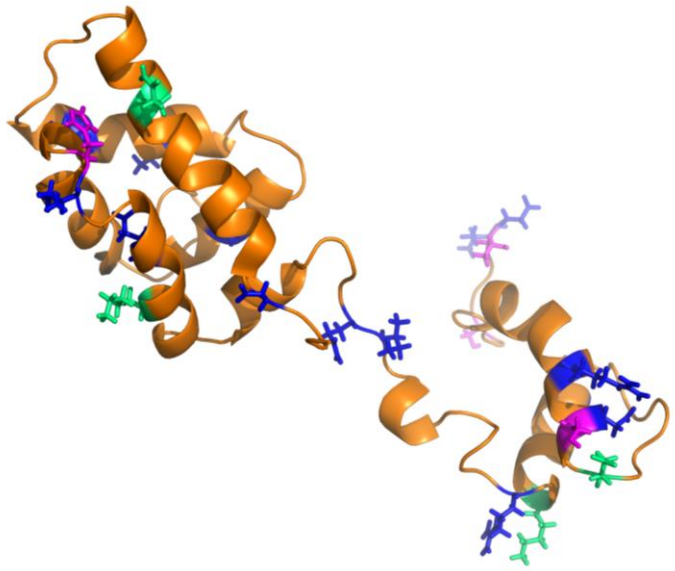

3

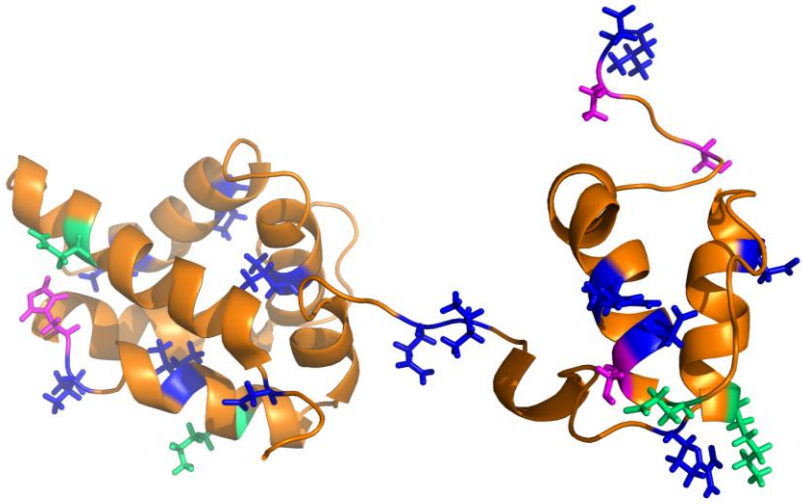

4

Figure 3.12 SDS gel electrophoresis of human Armet during expression and purification.

Lane 1: molecular mass markers.

Lane 2: *E. coli* cells with 1mM IPTG induction.

Lane 3: *E. coli* cells with 1mM IPTG induction (without mercaptoethanol).

Lane 4: Induced *E. coli* supernatant after sonication.

Lane 5: Induced *E. coli* supernatant after sonication (without mercaptoethanol).

Lane 6: Induced *E. coli* pellet after sonication.

Lane 7: Induced *E. coli* pellet after sonication (without mercaptoethanol).

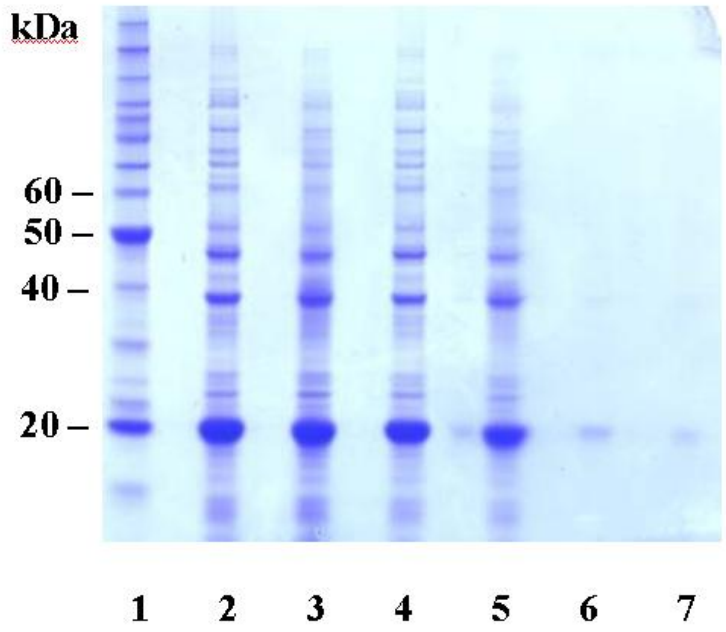
kDa
60 –
50 –
40 –
20 –
1
2
3
4
5
6
7

Figure 3.13 Western blot of Armet in expression and purification.

Lane 1: *E. coli* cells with 1mM IPTG induction.

Lane 2: *E. coli* cells with 1mM IPTG induction (without mercaptoethanol).

Lane 3: Induced *E. coli* supernatant after sonication.

Lane 4: Induced *E. coli* supernatant after sonication (without mercaptoethanol).

Lane 5: Induced *E. coli* pellet after sonication.

Lane 6: Induced *E. coli* pellet after sonication (without mercaptoethanol).

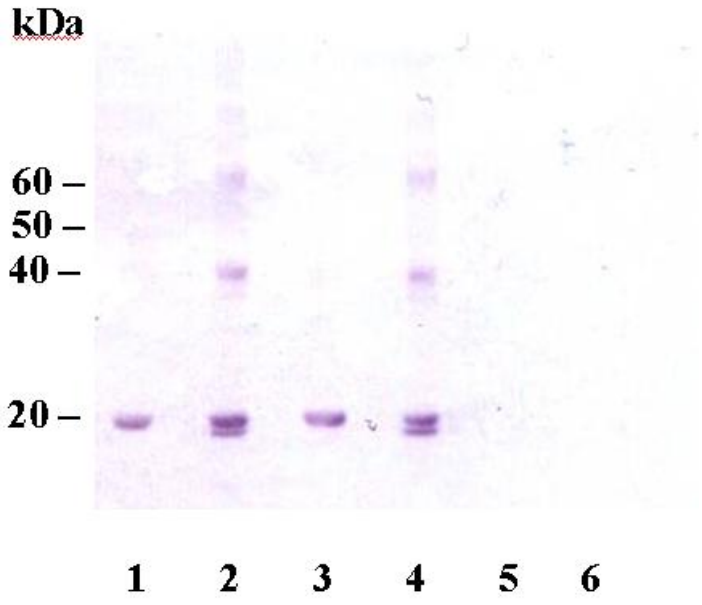
kDa
60 –
50 –
40 –
20 –
1
2
3
4
5
6

Figure 3.14 A plot of log MW vs relative mobility from western blot in Figure 3.13.

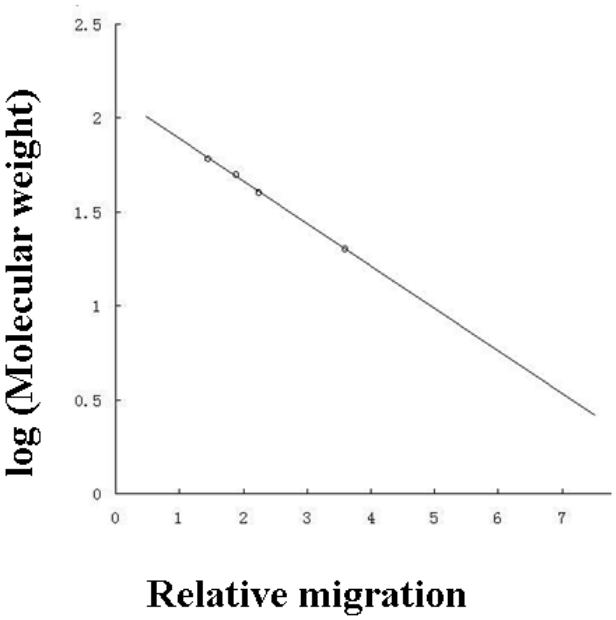
log (Molecular weight)
2.5
2
1.5
1
0.5
0
0
1
2
3
4
5
6
7
Relative migration

Figure 3.15 Armet mass determination by MALDI-TOF-MS.

Armet samples were prepared in 50 mM Tris-HCl, 100 mM NaCl, pH 7.0. Protein concentrations were 0.013 mM.

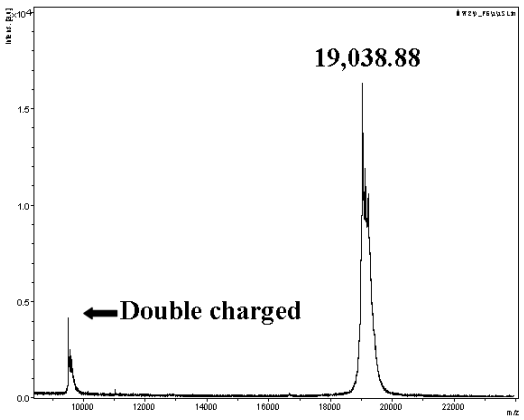
19,038.88
Double charged
10000
12000
14000
16000
18000
20000
22000
m/z

1

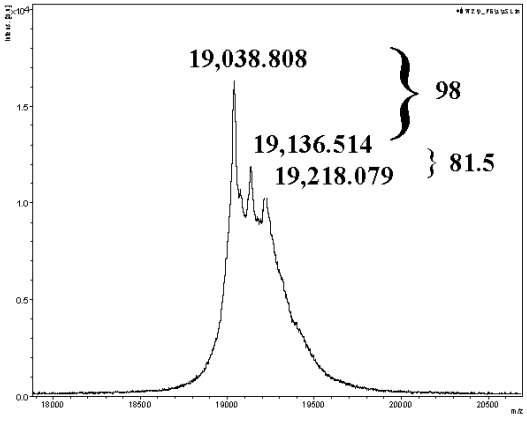
19,038.808
98
19,136.514
19,218.079
81.5
18000
18500
19000
19500
20000
20500
m/z

2

Figure 3.16 Armet mass determination by MALDI-TOF- MS.

The upper band and lower band were extracted from the SDS gel (Fig. 8, lane 8). MS spectra were collected for both bands.

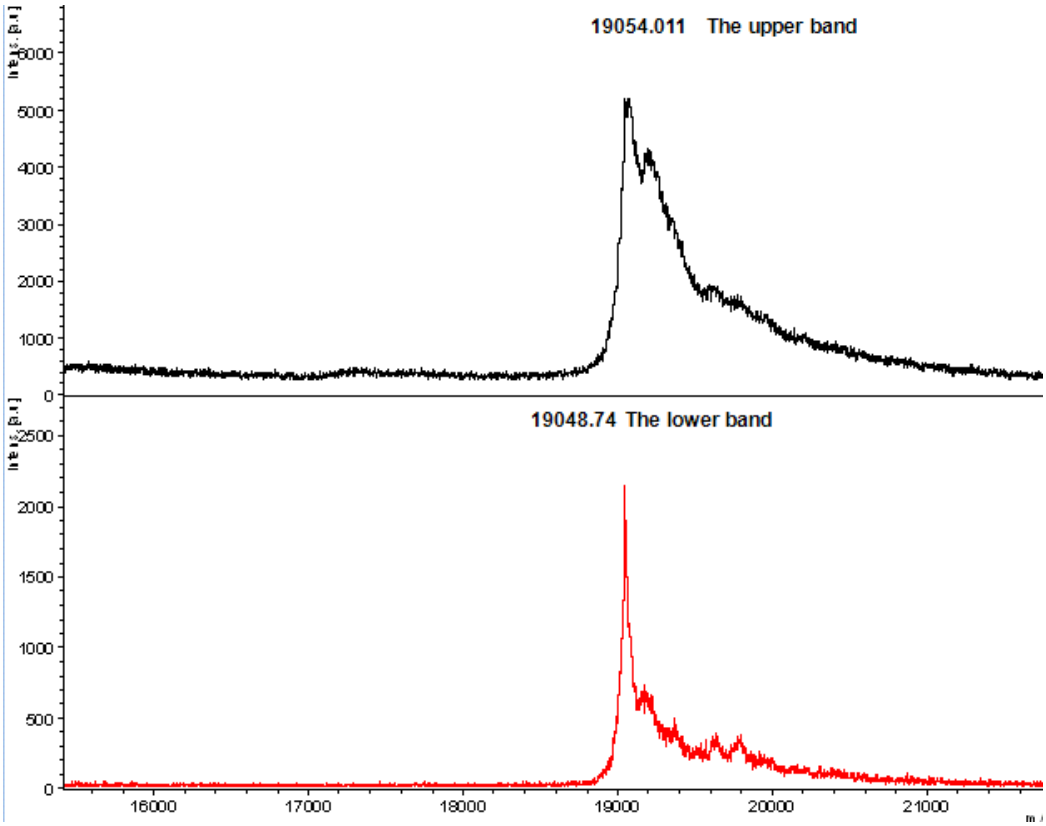
19054.011 The upper band
19048.74 The lower band
16000
17000
18000
19000
20000
21000

Figure 3.17 Sedimentation velocity experiments on Armet.

Buffer: 50 mM Tris, 100 mM NaCl, pH 7.0. Spectra were collected for Armet, Armet in the presence of DTT, and Armet in the presence of calcium.

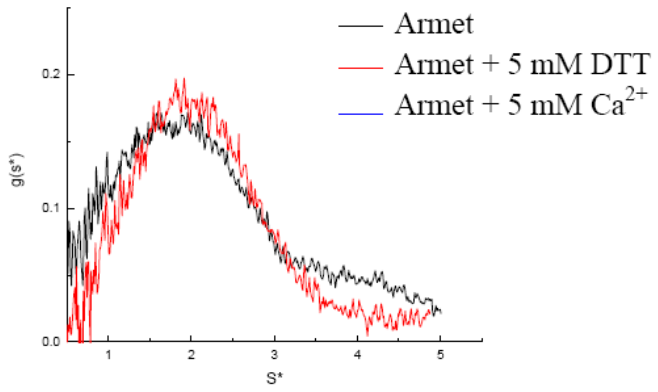
Armet
Armet + 5 mM DTT
Armet + 5 mM Ca2+
g(s*)
S*
0.0
0.1
0.2
1
2
3
4
5

1

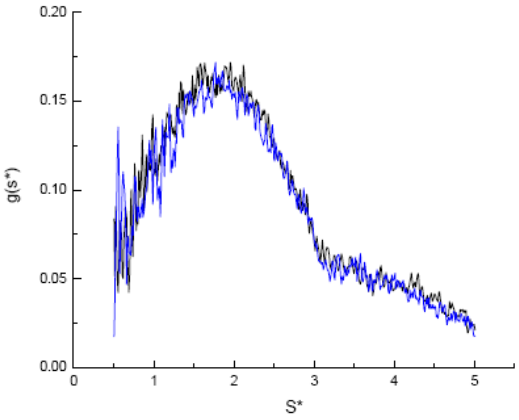
g(s*)
S*
0.00
0.05
0.10
0.15
0.20
0
1
2
3
4
5

2

Table 4.1 Disulfide bridges reported in human and mouse Armet.

	Human Armet	Mouse Armet
X-ray crystallography	**Cys6-C93, Cys9-C82, Cys40-Cys51, Cys127-Cys130 (Parkash et al., 2009)**	
NMR	**Cys6-Cys93, Cys9-Cys82, Cys40-Cys51, Cys127-Cys130 (Hellman et al., 2010)**	**Cys6-Cys93, Cys9-Cys82, Cys40-Cys51, Cys127-Cys130 (Hoseki et al., 2010)**
MALDI-TOF MS		**Cys6-Cys93, Cys9-Cys82, Cys40-Cys51, Cys127-Cys130 (Hoseki et al., 2010).** **Cys6-Cys9, Cys82-Cys93, Cys40-Cys51, Cys127-Cys130 (Mizobuchi et al., 2007)**

References

Airavaara M., Shen H., Kuo C. C., Peranen J., Saarma M., Hoffer B., and Wang Y. (2009). Mesencephalic astrocyte-derived neurotrophic factor reduces ischemic brain injury and promotes behavioral recovery in rats. The Journal of Comparative Neurology, 515, 116-124.

Apostolou A., Shen Y., Liang Y., Luo J., and Fang S. (2008). Armet, a UPR-regulated protein, inhibits cell proliferation and ER stress-induced cell death. Experimental Cell Research, 314, 2454-2467.

Evron E., Cairns P., Halachmi N., Ahrendt S. A., Reed A. L., and Sidransky D. (1997) Normal polymorphism in the incomplete trinucleotide repeat of the arginine-rich protein gene. Cancer Research, 57, 2888-2889.

Fernandez P. M., Overexpression of the glucose-regulated stress gene GRP78 in malignant but not benign human breast lesions. Breast Cancer Res Treat, 59(1), 15-26.

Halsall H. B. and Wermeling J. R. (1982). Sedimentation coefficient, frictional coefficient, and molecular weight. Journal of Chemical Education, 59(12), 1076-1078.

Healy S. J. M., Gorman A. M., Mousavi-Shafaei P., Gupta S. and Samali A. (2009). Targeting the endoplasmic reticulum-stress response as an anticancer strategy. European Journal of Pharmacology, 625, 234-246.

Hebenstreit D. and Ferreira F. (2005). Structural changes in calcium-bindings allergens: use of circular dichroism to study binding characteristics. Allergy, 60, 1208-1211.

Hellman M., Arumae U., Yu L. Y., Lindholm P., Peranen J., Saarma M., and Permi P. (2010). Neurotrophic factor MANF has a unique mechanism to rescue apoptotic neurons. Journal of Biological Chemistry, 286(10), 2675-2680.

Hellman M., Peranen J., Saarma M., and Permi P. (2010). ^{1}H, ^{13}C and ^{15}N resonance assignments of the human mesencephalic astrocyte-derived neurotrophic factor. Biomol NMR Assign, 4(2), 215-217.

Hoseki J., Sasakawa H., Yamaguchi Y., Maeda M., Kubota H., Kato K., and Nagata K. (2010). Solution structure and dynamics of mouse ARMET. FEBS Letters, 584, 1536-1542.

Kim I., Xu W., and Reed J. C. (2008). Cell death and endoplasmic reticulum stress: disease relevance and therapeutic opportunities. Nature Reviews Drug Discovery, 7, 1013-1030.

Lindholm P., Peranen J., Andressoo J. O., Kalkkinen N., Kokaia Z., Lindvall O., Timmusk T., and Saarma M. (2008). MANF is widely expressed in mammalian tissues and differently regulated after ischemic and epileptic insults in rodent brain. Molecular and Cellular Neuroscience, 39(3), 356-371.

Lindholm P., Voutilainen M. H., Lauren J., Peranen J., Leppanen V. M., Andressoo J. O., Lindahl M., Janhunen S., Kalkkinen N., Timmusk T., Tuominen R. K., and Saarma M. (2007). Novel neurotrophic factor CDNF protects and rescues midbrain dopamine neuron *in vivo*. Nature, 448(5), 73-77.

Ma Y., Hendershot L. M. (2004). The role of the unfolded protein response in tumor development: friend or foe? Nature Reviews Cancer, 4, 966-977.

Mani, R. S., Boyes B. E., and Kay C. M. (1982). Physicochemical and optical studies on calcium- and potassium-induced conformational changes in bovine brain S-100b protein. Biochemistry, 21, 2607-2612.

Mizobuchi N., Hoseki J., Kubota H., Toyokuni S., Nozaki J., Naitoh M., Koizumi A., and Nagata K. (2007). Armet is a soluble ER protein induced by the Unfolded Protein Response *via* ERSE-II element. Cell Structure and Function, 32, 41-50.

Michalak M., Robert Parker J. M., and Opas M. (2002). Ca^{2+} signaling and calcium binding chaperones of the endoplasmic reticulum. Cell Calcium, 32(5-6), 269-278.

Parkash V., Lindholm P., Peranen H., Kalkkinen N., Oksanen E., Saarma M., Leppanen V. M., and Goldman A. (2009). The structure of the conserved neurotrophic factors MANF and CDNF explains why they are bifunctional. Protein Engineering, Design & Selection, 22(4), 233-241.

Petrova P. S., Raibekas A., Pevsner J., Vigo N., Anafi M., Moore M. K., Peaire A. E., Shridhar V., Smith D. I., Kelly J., Durocher Y., and Commissiong J. W. (2003). A new mesencephialic, astrocyte-derived neurotrophic factor with selectivity for dopaminergic neurons. Journal of Molecular Neuroscience, 20, 173-187.

Raykhel I., Alanen H., Salo K., Jurvansuu J., Nguyen V. D., Latva-Ranta M., and Ruddock L. (2007). A molecular specificity code for the three mammalian KDEL receptors. The Journal of Cell Biology, 179, 1193-1204.

Romero-Ramirez L., Cao H., Nelson D., Hammond E., Lee AH., Yoshida H., Mori K., Glimcher LH., Denko NC., Giaccia AJ., Le QT., and Koong AC. XBP1 is essential for survival under hypoxic conditions and is required for tumor growth. Cancer Res, 64(17), 5943-5947.

Shroder M. and Kaufman R. J. (2005). The mammalian unfolded protein response. Annu. Rev. Biochem, 74, 739-789.

Shuda M., Kondoh N., Imazeki N., Tanaka K., Okada T., Mori K., Hada A., Arai M., Wakatsuki T., Matsubara O., Yamamoto N., and Yamamoto M. (2003). Activation of the ATF6, XBP1 and grp78 genes in human hepatocellular carcinoma: a possible involvement of the ER stress pathway in hepatocarcinogenesis. J. Hepatol, 38, 605-614.

Song M. S., Park Y. K., Lee J. H., and Park K. (2001). Induction of glucose-regulated protein 78 by chronic hypoxia in human gastric tumor cells through a protein kinase C-ε/ERK/AP-1 signaling cascade. Cancer Res, 61, 8322-8330.

Tadimalla A., Belmont P. J., Thuerauf D. J., Glassy M. S., Martindale J. J., Gude N., Sussman M. A., and Glembotski C. C. (2009). Mesencephalic astrocyte-derived neurotrophic factor is an ischemia-inducible secreted endoplasmic reticulum stress response protein in the heart. Circulation Research, 103, 1249-1258.

Verkhratsky A. and Toescu E. C. (2003). Endoplasmic reticulum Ca^{2+} homeostasis and neuronal death. J. Cell. Mol. Med, 7(4), 351-361.

Voutilainen M. H., Back S., Porsti E., Toppinen L., Lindgren L., Lindholm P., Peranen J., Saarma M., and Tuominen R. K. (2009). Mesencephalic astrocyte-derived neurotrophic factor is neurorestrorative in rat model of parkinson's disease. The Journal of Neuroscience, 29(30), 9651-9659.

Wijeyesakere S. J., Gafni A. A., and Raghavan M. (2010). Calreticulin is a thermostable protein with distinct structural responses to different divalent cation environments. The Journal of Biological Chemistry, published on December 22, 2010 as Manuscript M110.169193.

Yu Y. Q., Liu L. C., Wang F. C., Liang Y., Cha D. Q., Zhang J. J., Sheng Y. J., Wang H. P., Fang S. Y., and Shen Y. X. (2010). Induction profile of MANF/ARMET by cerebral ischemia and its implication for neuron protection. Journal of Cerebral Blood Flow & Metabolism, 20, 79-91.

Appendix A - Supplementary data

Sphingomyelin binding of Armet studied by NMR

2D ^{1}H-^{15}N HSQC spectra were recorded for Armet in the presence (3 mM) and in the absence of sphingomyelin (Fig. A. 1, Fig. A. 2). After sphingomyelin binding, changes of chemical shift were observed in Glu100 and Leu158. Residues with decreased signal strength included Gln18, Arg41, Asn66, Gln91, Gln100, Lys109, Leu111, Asp115, Lys118, Trp123, Cys130, Glu132, Asn141, Leu143, Lys146, Arg155, and Glu157 (Fig. A. 3, Fig. A. 4).

HSQC NMR spectra of Armet in different conditions

2D ^{1}H-^{15}N HSQC spectra of Armet were recorded with different buffer condition and with different potential chemical ligands. No significant changes in spectra were detected after adding cefoperazone (Fig. A.8, Fig. A.9) or aminophenazone (Fig. A.10, Fig. A.11) to Armet sample. It indicates there is no binding between Armet and these chemicals.

Calcium binding of Armet studied by isothermal titration calorimetry (ITC)

Calcium binding of Armet was studied by ITC (Fig. A.13). Data fitting by using “Origin for ITC” software (Fig. A.13) suggests two binding sites. Binding constants for one site is in milimolar range and for the other one is in micromolar range. Both hypothetical binding sites bind one calcium ion.

Figure A.1 2D ^{1}H-^{15}N HSQC spectrum of Armet.

Buffer: 25 mM Tris-HCl, pH 7.0. Protein concentration was 0.3 mM. Spectrum was recorded at 35℃.

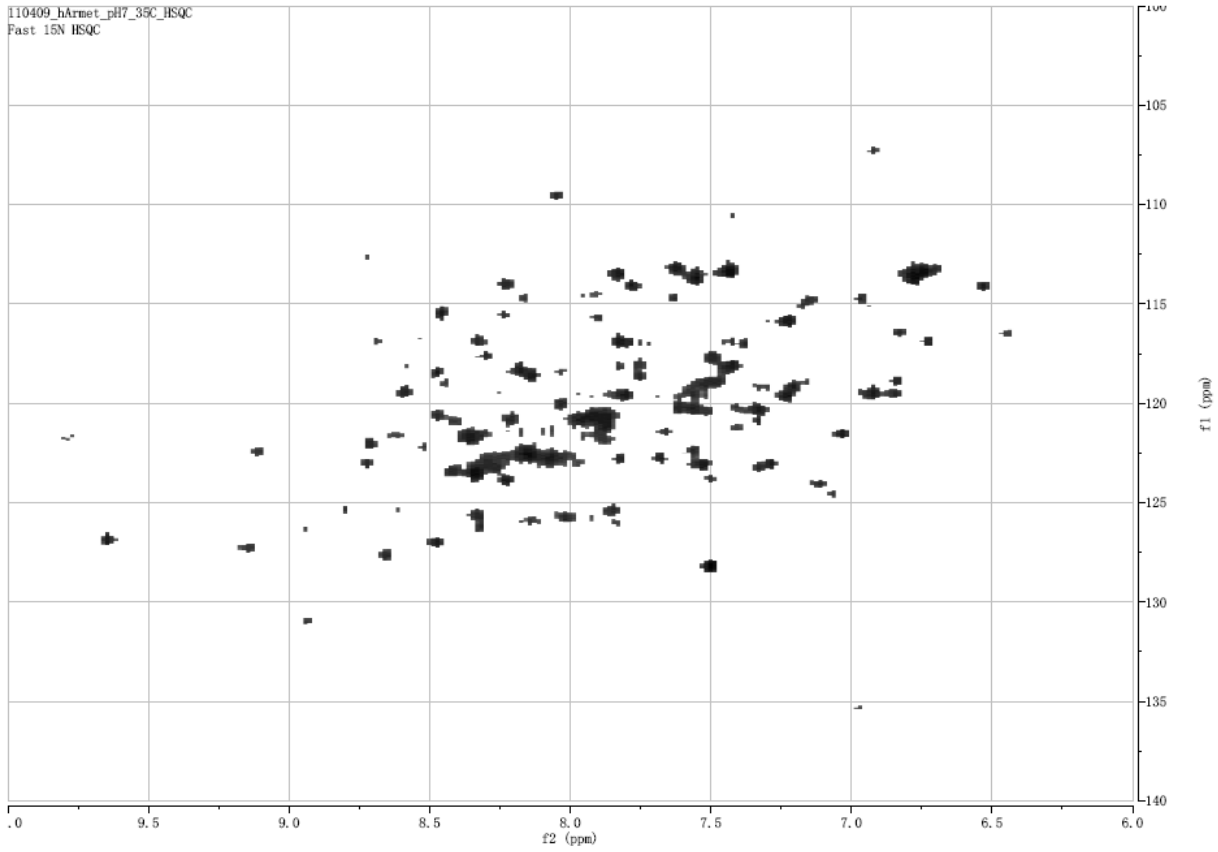
110409_hArmet_pH7_35C_HSQC
Fast 15N HSQC
105
110
115
120
125
130
135
140
f1 (ppm)
9.5
9.0
8.5
8.0
7.5
7.0
6.5
6.0
f2 (ppm)

Figure A.2 2D ^{1}H-^{15}N HSQC spectrum of sphigomyelin-bound Armet.

Buffer: 25 mM Tris-HCl, pH 7.0. Protein concentration was 0.3 mM. Spectrum was recorded at 35℃. Sphingomyelin concentration was 3 mM.

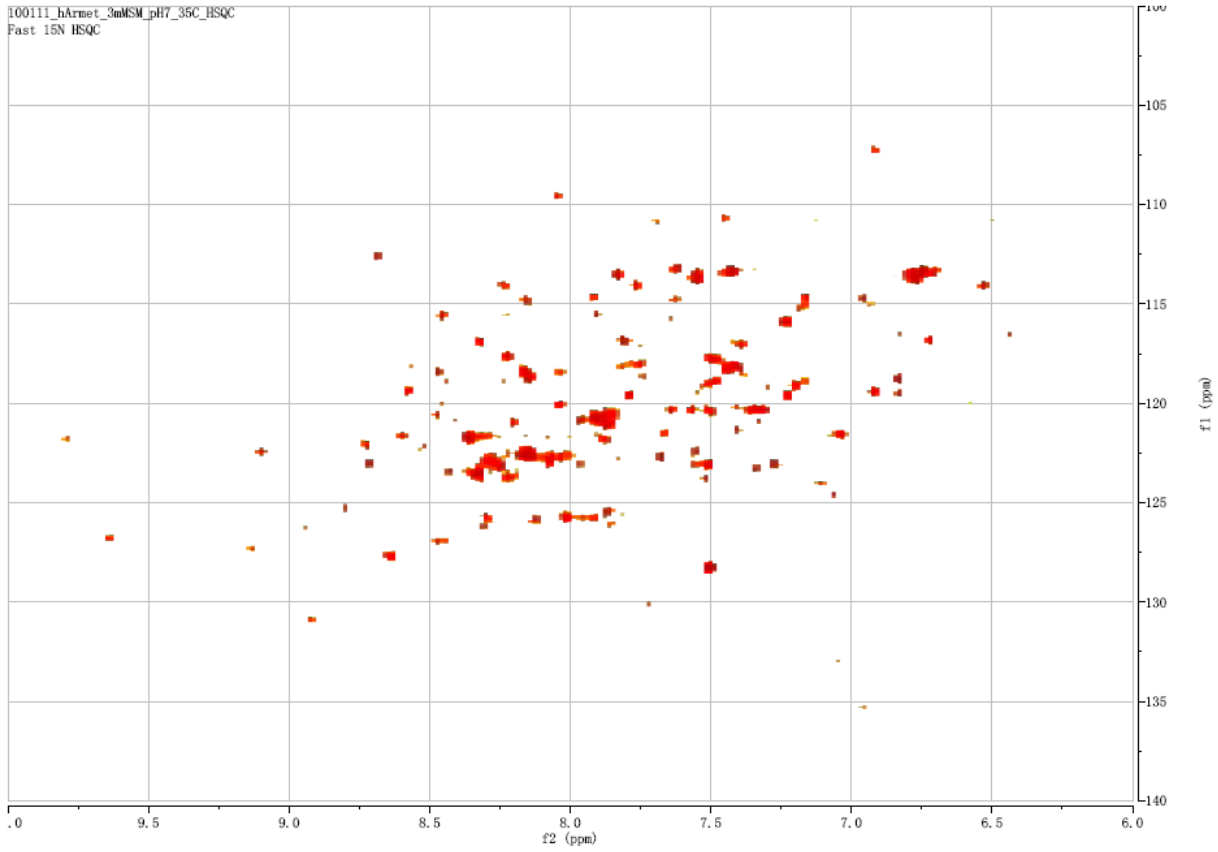
100111_hArmet_3mMSM_pH7_35C_HSQC
Fast 15N HSQC
105
110
115
120
125
130
135
140
f1 (ppm)
9.5
9.0
8.5
8.0
7.5
7.0
6.5
6.0
f2 (ppm)

Figure A.3 Overlaid 2D ^{1}H-^{15}N HSQC spectra of Armet in the absence and in the presence of sphingomyelin.

Black: Armet without sphingomyelin.

Red: Armet with sphingomyelin.

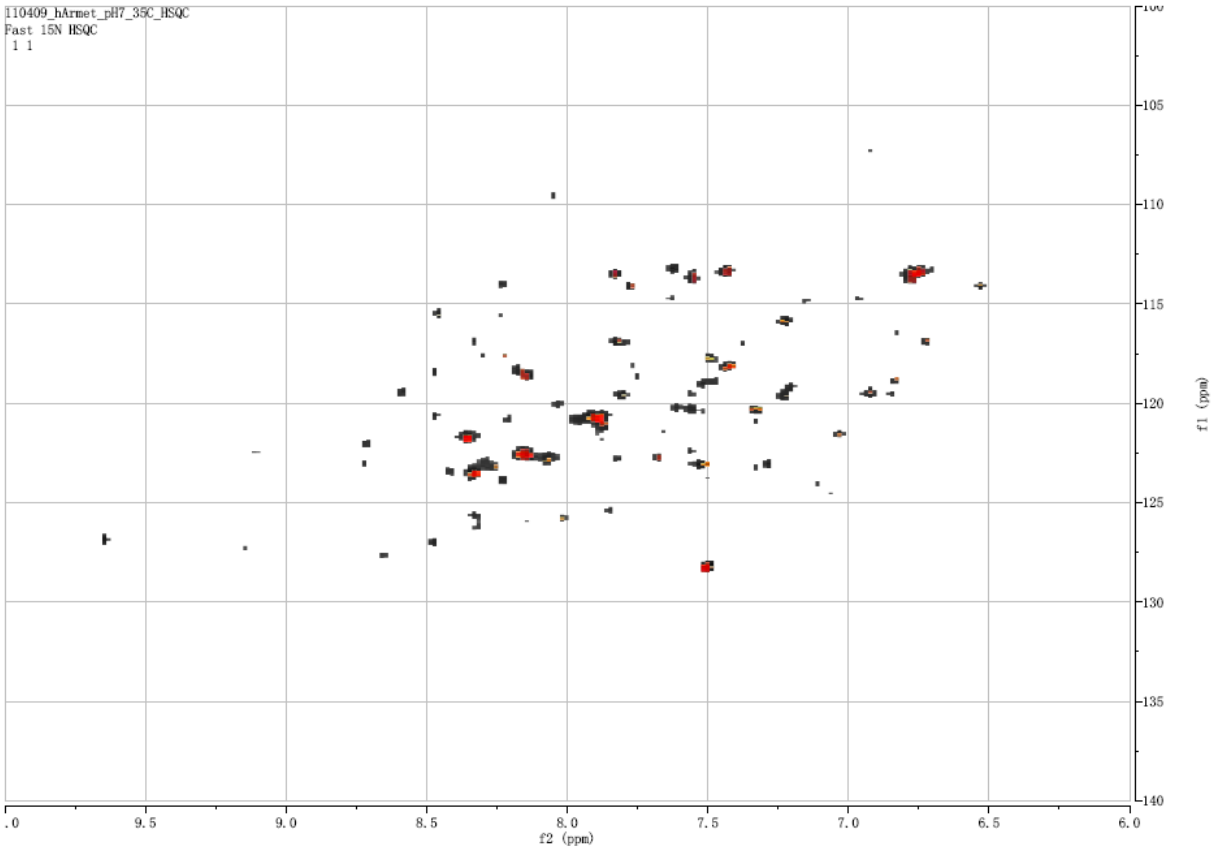
110409_hArmet_pH7_35C_HSQC
Fast 15N HSQC
1 1
105
110
115
120
125
130
135
140
f1 (ppm)
9.5
9.0
8.5
8.0
7.5
7.0
6.5
6.0
f2 (ppm)

Figure A.4 2D ^{1}H-^{15}N HSQC difference spectrum of Armet.

Blue: Peaks with decreased signal strength in the presence of sphingomyelin.

Red: Peaks with increased signal strength in the presence of sphingomyelin.

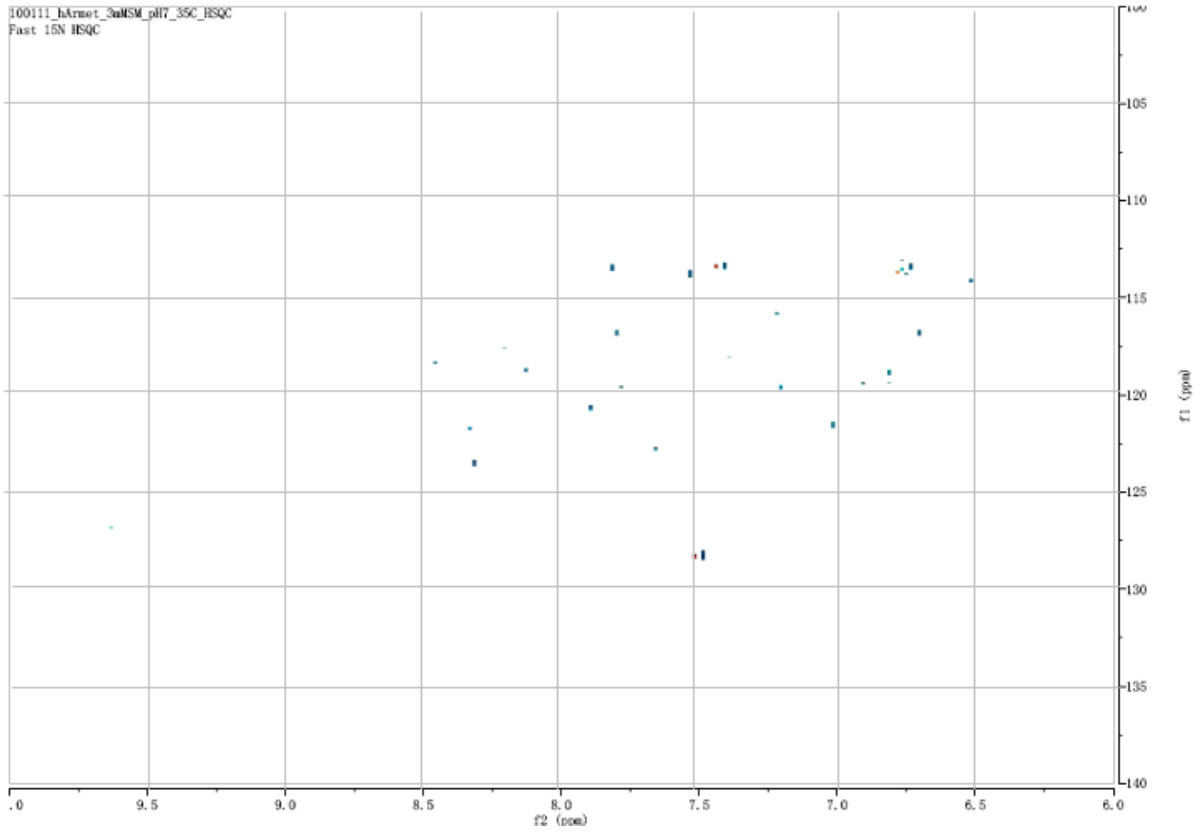
100111_hArmet_2mMSM_pH7_35C_HSQC
Fast 15N HSQC
105
110
115
120
125
130
135
140
f1 (ppm)
.0
9.5
9.0
8.5
8.0
7.5
7.0
6.5
6.0
f2 (ppm)

Figure A.5 2D ^{1}H-^{15}N HSQC difference spectrum of Armet.

Blue: Peaks with decreased signal strength in the presence of sphingomyelin.

Red: Peaks with increased signal strength in the presence of sphingomyelin.

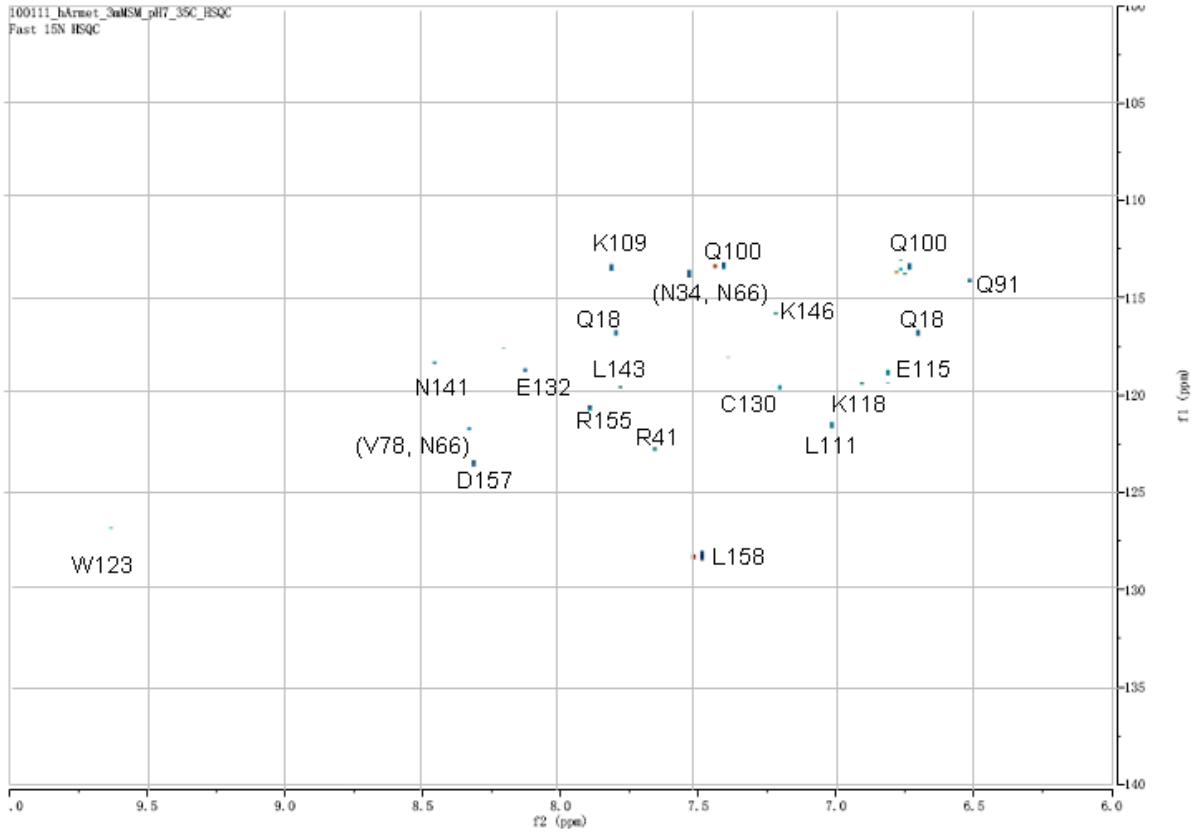
100111_hArmet_2mMSM_pH7_35C_HSQC
Fast 15N HSQC
K109
Q100
(N34, N66)
Q100
Q91
Q18
K146
Q18
L143
E115
N141
E132
C130
K118
R155
R41
L111
(V78, N66)
D157
W123
L158
f2 (ppm)
f1 (ppm)

Figure A.6 Residues in Armet with changed 2D ^{1}H-^{15}N HSQC signals in the presence of sphingomyelin.

Perturbed amino acid residues are blue.

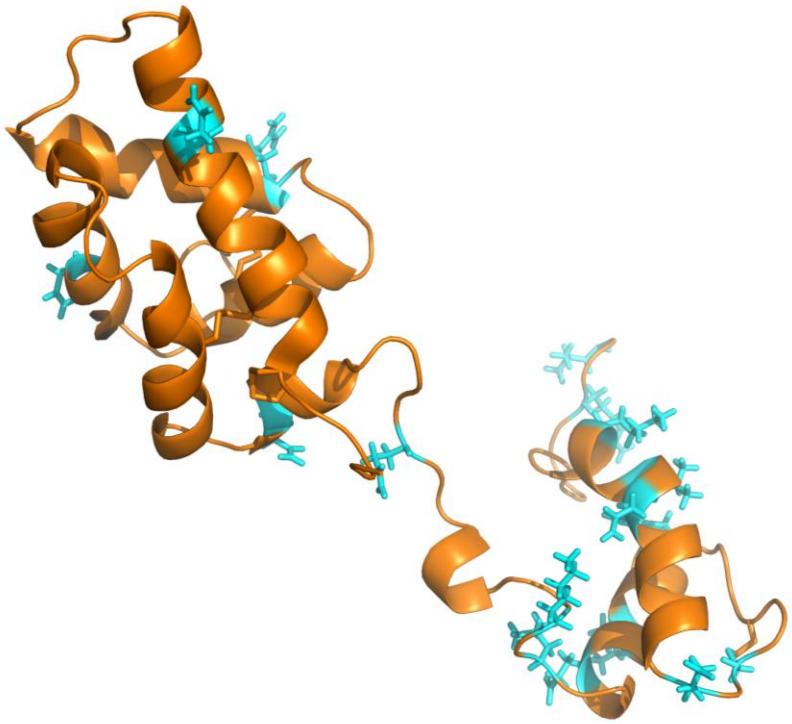

Figure A.7 Perturbed Asp and Glu residues are conserved in Armets.

N-terminal secretion signals are blue. C-terminal ER retention signals are pink. Conserved Cysteines are yellow. Perturbed Asp and Glu residues are green.


H. sapiens MWATQGL-AVALA-LSVLP-G-SRALRPGDCEVCISYLGRFYQDLKDRDVTFSPATIENE 56
M. musculus MWATRGL-AVALA-LSVLP-D-SRALRPGDCEVCISYLGRFYQDLKDRDVTFSPATIEEE 56
R. norvegicus MWATRGL-AVALA-LSVLP-D-SRALRPGDCEVCISYLGRFYQDLKDRDVTFSPATIEEE 56
S. scrofa MWFTHGL-AVALA-LSVLP-A-SRALRPGDCEVCISYLGRFYQDLKDRDVTFSPASIEKE 56
B. taurus MWATHGL-AVALA-LSVLP-A-SRALRQGDCEVCISYLGRFYQDLKDRDVTFSPASIEKE 56
X. tropicalis M-VPLALITVTGM-LALLPSD-AAALKAGDCEVCISFMTRLYQSLKERKVEFKPDVVEKE 57
S. salar MLCLSSL-SVALAVLALVPSS-SDALKDGECEVCVSFLGRFYQSLQDNHVKFTSADIEKE 58
O. mordax MLCLSGL-SVALA-LTLVPSS-TDALKEGDCEVCVGFLGKFYQLLQEEDVKFDSTAIEKA 57
C. elegans MSR---L--VLLISLVIVV-A-SAAAPQ--CEVCKKVLDDVMAKVPAGD-KSKPDAIGKV 50
A. pisum MDKHILLVCVFFIVFHVFQAQ-SRTFTEEDCPVCVLTIDKFSKTL-EG--ELNPKNIEEQ 56
D. melanogaster M-KTWYMVVV--IGFLATLAQTSLALKEEDCEVCVKTVRRFADSL-DDSTKKDYKQIETA 56
C. clemensi MWK--VLLCLL-VAF-VADSG-VFSLKEGECEVCVSVLNRFKETLSKGD-ASSPPAIEKG 54
H. sapiens LIKFCREAR-GKENRLCYYIGATDDAATKIINEVSKPLAHHIPVEKIC-EKLKKKDSQIC 114
M. musculus LIKFCREAR-GKENRLCYYIGATDDAATKIINEVSKPLAHHIPVEKIC-EKLKKKDSQIC 114
R. norvegicus LIKFCREAR-GKENRLCYYIGATDDAATKIINEVSKPLAHHIPVEKIC-EKLKKKDSQIC 114
S. scrofa LTKFCREAR-GKENRLCYYIGATDDAATKIINEVSKPLAHHIPVEKIC-EKLKKKDSQIC 114
B. taurus LIKFCREAR-GKENRLCYYIGATEDAATKIINEVSKPLSHHIPVEKIC-EKLKKKDSQIC 114
X. tropicalis LLKTCNDAR-GKENRLCYYIGATSDAATKITNEVSRPLSNHIPPEKIC-EKLKKKDGQIC 115
S. salar LVKTCKDVK-GKENRFCYYIGGTNDAATKILNEISKPLSYHTPVDKIC-EKLKKKDSQIC 116
O. mordax LVKSCKDAR-GKDNRFCYYIGATSDAATKIINEISKPLSYHVPVEKIC-EKLKKKDSQIC 115
C. elegans IREHCETTR-NKENKFCFYIGALPESATSIMNEVTKPLSWSMPTEKVCLEKLKGKDAQIC 109
A. pisum FKKYCLSTKIDKEKRLCYYLGGLEDSATGILSEMSKPLSWSMPALKIC-ERLKKMDAQVC 115
D. melanogaster FKKFCKAQK-NKEHRFCYYLGGLEESATGILNELSKPLSWSMPAEKIC-EKLKKKDAQIC 114
C. clemensi FRKFCKDLK-LKENRFCYYLGGTEDAATGILGEMSKPLSWGMPVLKVC-EKLEKKDRQIC 112
H. sapiens ELKYDKQIDLSTVDLKKLRVKELKKILDDWGETCKGCAEKSDYIRKINELMPKYAPKAAS 174
M. musculus ELKYDNQIDLSTVDLKKLRVKELKKILDDWGEMCKGCAEKSDYIRKINELMPKYAPKAAS 174
R. norvegicus ELKYDKQIDLSTVDLKKLRVKELKKILDDWGEMCKGCAEKSDYIRKINELMPKYAPKAAS 174
S. scrofa ELKYDKQIDLSTVDLKKLRVKELKKILDDWGETCKGCAEKSDYIRKINELMPKYAPKAAS 174
B. taurus ELKYDKQIDLSTVDLKKLRVKELKKILDDWGETCKGCAEKSDYIRKINELMPKYAPKAAS 174
X. tropicalis ELKYDKQIDLSTVDLKKLKVKELKKILDDWGESCKGCAEKSDFIRKINELMPKYAPNAAN 175
S. salar ELKYDKQVDLSTVDLKKLKVKDLKKILEEWGESCKGCAEKSDFIRKINELMPKYAPNAAQ 176
O. mordax ELKYDKQVDLSTVDLKKLKVKDLKKILEEWGETCKGCAEKSDFIRKINELMPKYAPNAAK 175
C. elegans ELKYDKPLDWKTIDLKKMRVKELKNILGEWGEVCKGCTEKAELIKRIEELKPKYV----- 164
A. pisum DIKYDKEIDWKTVNLKKMKVKDLKKILDNWGEICDGCLEKTDYIKRVEELKPSYV----- 170
D. melanogaster DLRYEKQIDLNSVDLKKLKVRDLKKILNDWDESCDGCLEKGDFIKRIEELKPKYS----- 169
C. clemensi ELRYDKQIDLKNVNLKKLKVRDLKKILNDWDEICDGCLEKADFIKRIEELKPKYM----- 167

H. sapiens	ARTDL	179
M. musculus	ARTDL	179
R. norvegicus	ARTDL	179
S. scrofa	SRTDL	179
B. taurus	SRTDL	179
X. tropicalis	ARTDL	180
S. salar	ARTDL	181
O. mordax	ARTEL	180
C. elegans	-KEEL	168
A. pisum	-KEEL	174
D. melanogaster	-RSEL	173
C. clemensi	-REGL	171
	: *	

Figure A.8 2D ^{1}H-^{15}N HSQC spectrum of Armet with cefoperazone.

Buffer: 50 mM BisTris, 150 mM NaCl, pH 6.5. Protein concentration was 0.3 mM. Cefoperazone concentration was 3 mM.

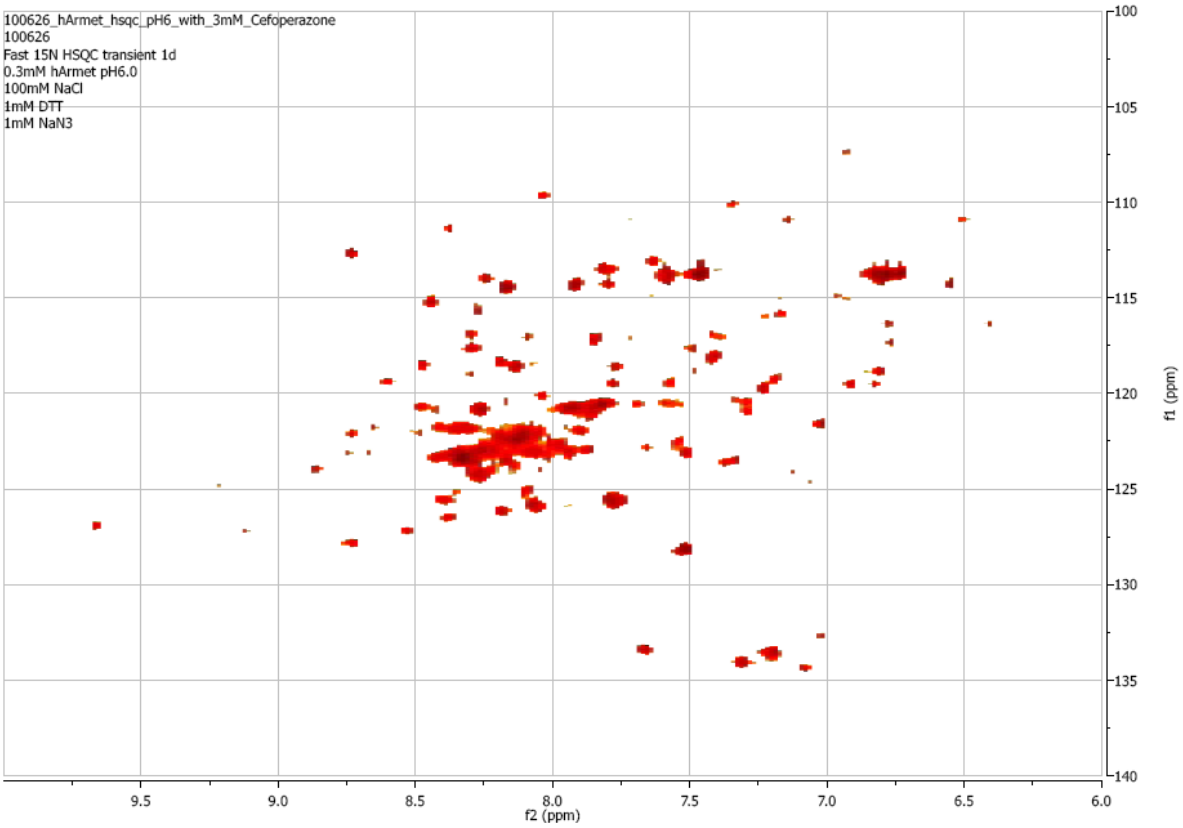
100626_hArmet_hsqc_pH6_with_3mM_Cefoperazone
100626
Fast 15N HSQC transient 1d
0.3mM hArmet pH6.0
100mM NaCl
1mM DTT
1mM NaN3
f2 (ppm)
f1 (ppm)

Figure A.9 2D ^{1}H-^{15}N HSQC difference spectrum of Armet with cefoperazone.

Blue: Peaks with decreased signal strength in the presence of cefoperazone.

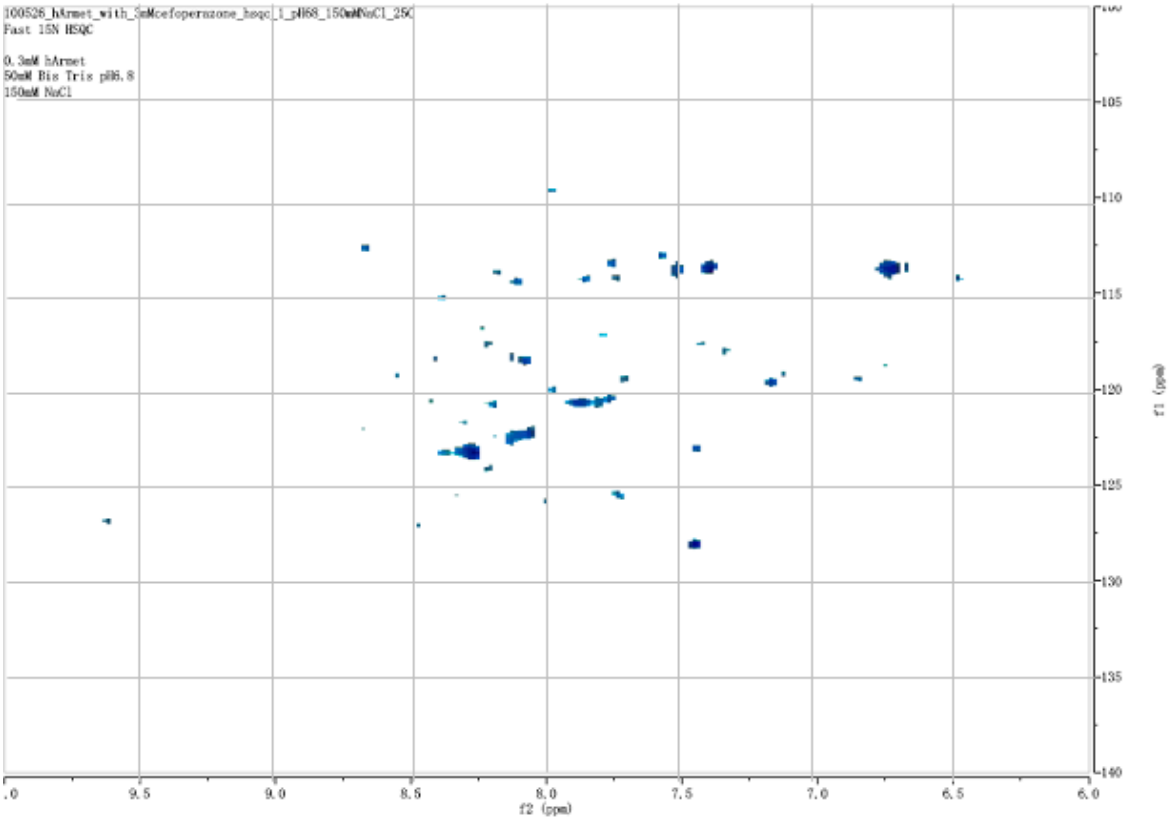
Fast 15N HSQC
0.3mM hArmet
50mM Bis Tris pH6.8
150mM NaCl
105
110
115
120
125
130
135
140
f1 (ppm)
.0
9.5
9.0
8.5
8.0
7.5
7.0
6.5
6.0
f2 (ppm)

Figure A.10 2D ^{1}H-^{15}N HSQC spectrum of Armet with Aminophenazone.

Buffer: 50 mM BisTris, 150 mM NaCl, pH 6.5. Protein concentration was 0.3 mM. Aminophenazone concentration was 3 mM.

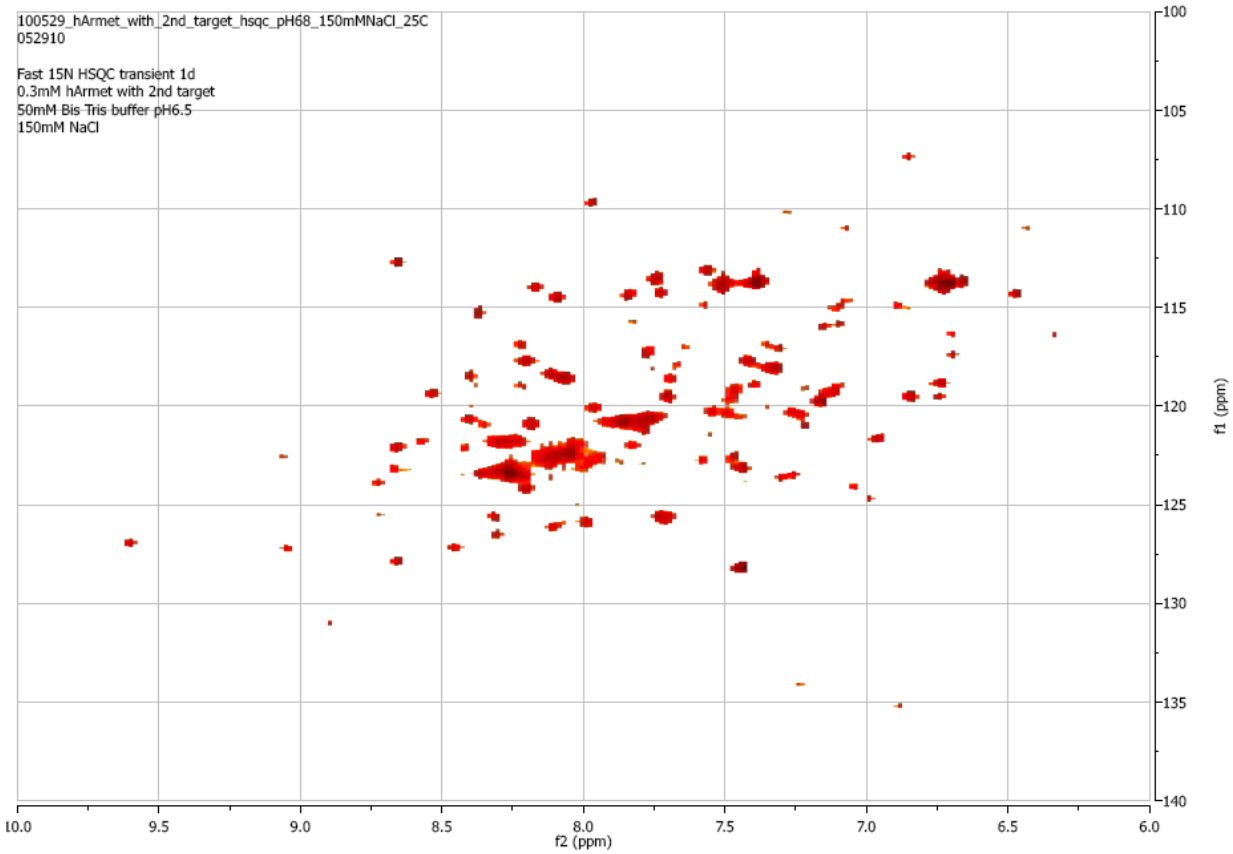
100529_hArmet_with_2nd_target_hsqc_pH68_150mMNaCl_25C
052910
Fast 15N HSQC transient 1d
0.3mM hArmet with 2nd target
50mM Bis Tris buffer pH6.5
150mM NaCl
100
105
110
115
120
125
130
135
140
f1 (ppm)
10.0
9.5
9.0
8.5
8.0
7.5
7.0
6.5
6.0
f2 (ppm)

Figure A.11 2D ^{1}H-^{15}N HSQC difference spectrum of Armet with aminophenazone.

Blue: Peaks with decreased signal strength in the presence of Aminophenazone.

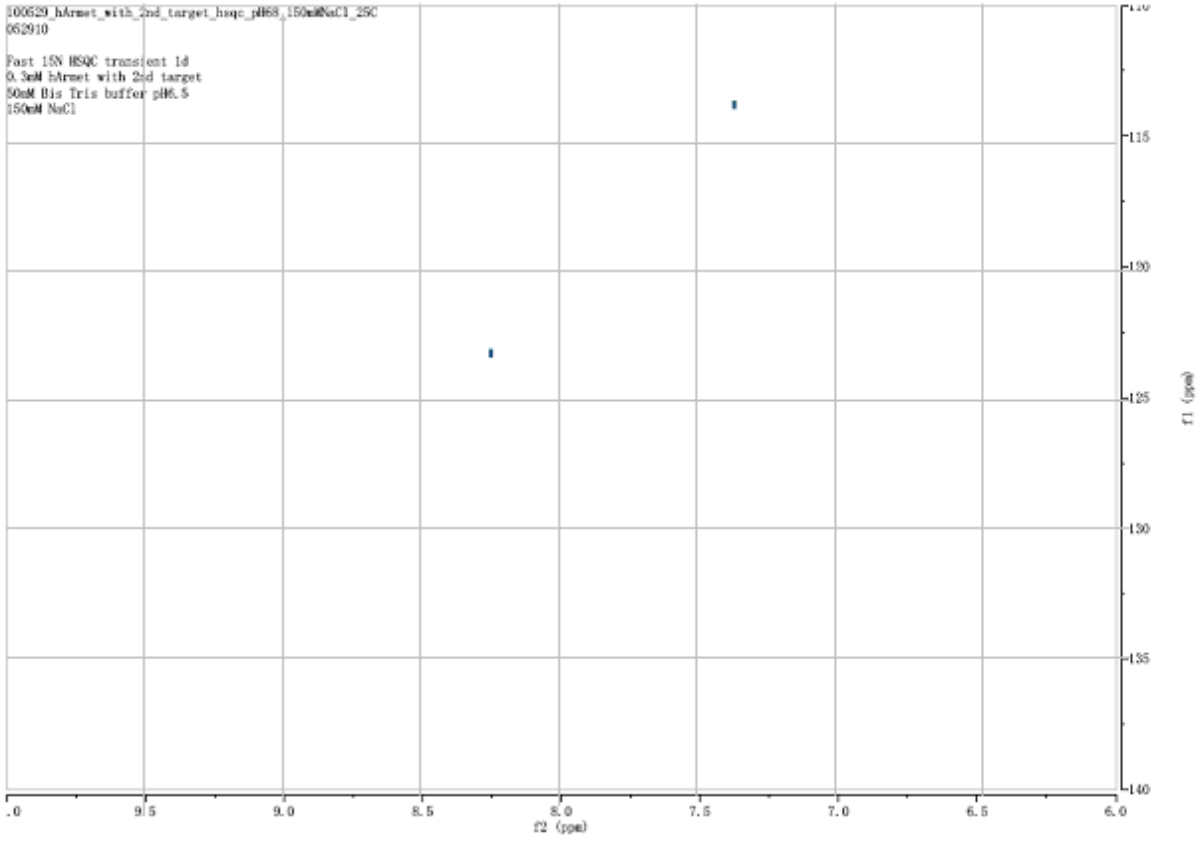
100529_hArmet_with_2nd_target_hsqc_pH68_150mMNaCl_25C
062910
Fast 15N HSQC transient 1d
0.3mM hArmet with 2nd target
50mM Bis Tris buffer pH6.5
150mM NaCl
f1 (ppm)
f2 (ppm)

Figure A.12 2D ^{1}H-^{15}N HSQC spectrum of ^{15}N, ^{13}C labeled Armet.

Buffer: 25 mM Na_2HPO_4, 150 mM NaCl, pH 6.5. Protein concentration was 0.4 mM. Spectrum was recorded at 25℃.

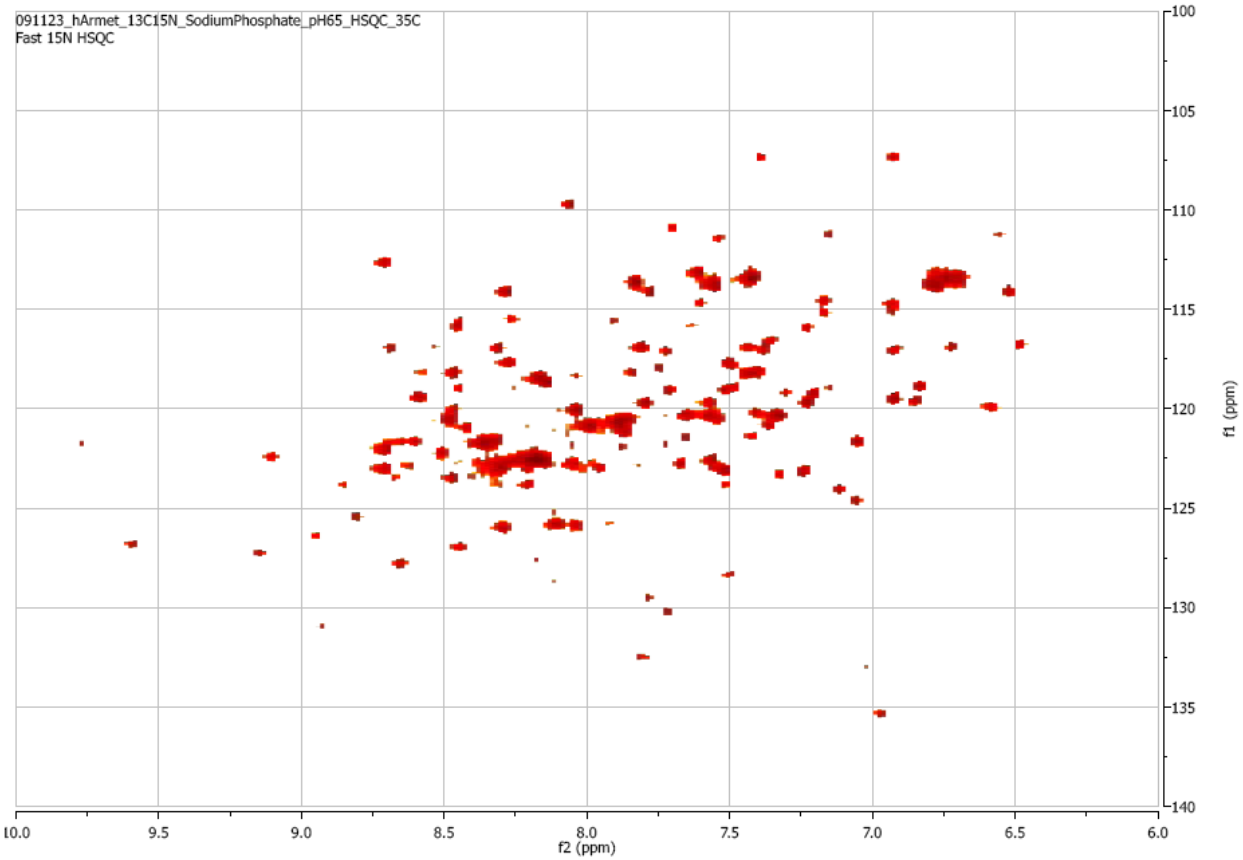
091123_hArmet_13C15N_SodiumPhosphate_pH65_HSQC_35C
Fast 15N HSQC
100
105
110
115
120
125
130
135
140
f1 (ppm)
10.0
9.5
9.0
8.5
8.0
7.5
7.0
6.5
6.0
f2 (ppm)

Figure A.13 Calcium binding of Armet studied by isothermal titration calorimetry (ITC).

Buffer: 50 mM Tris-HCl, 100 mM NaCl, pH 7. Protein concentration was 0.07 mM.

(1): Titration of Armet with calcium.

(2): Two binding sites data fitting of calcium binding.

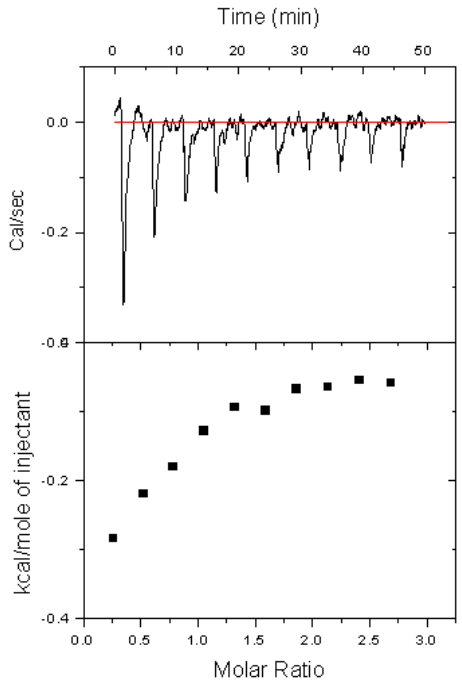
Time (min)
0
10
20
30
40
50
0.0
-0.2
-0.4
Cal/sec
kcal/mole of injectant
-0.2
-0.4
0.0
0.5
1.0
1.5
2.0
2.5
3.0
Molar Ratio

1

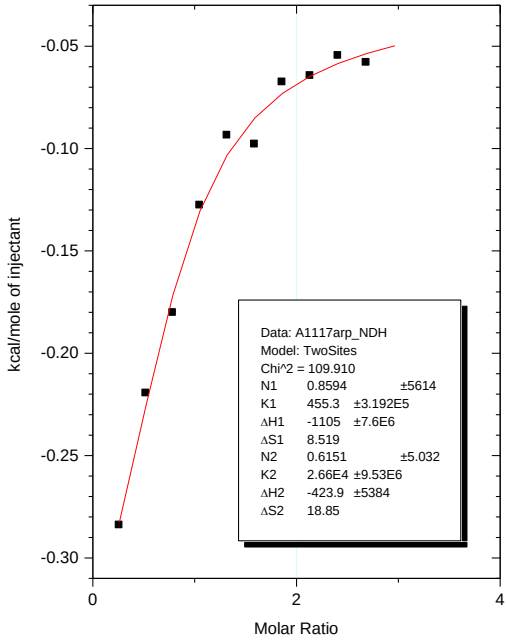
-0.05
-0.10
-0.15
-0.20
-0.25
-0.30
kcal/mole of injectant
0
2
4
Molar Ratio
Data: A1117arp_NDH
Model: TwoSites
Chi^2 = 109.910
N1 0.8594 ±5614
K1 455.3 ±3.192E5
ΔH1 -1105 ±7.6E6
ΔS1 8.519
N2 0.6151 ±5.032
K2 2.66E4 ±9.53E6
ΔH2 -423.9 ±5384
ΔS2 18.85

2